# Send-receive communication asymmetry in brain networks: Inferring directionality of neural signalling from undirected structural connectomes

Caio Seguin[1],* Adeel Razi[2,3,4], and Andrew Zalesky[1,5]
[1] *Melbourne Neuropsychiatry Centre, The University of Melbourne and Melbourne Health, Melbourne, VIC 3010, Australia*
[2] *Monash Institute of Cognitive and Clinical Neurosciences, and Monash Biomedical Imaging, Monash University, Clayton, Australia*
[3] *The Wellcome Trust Centre for Neuroimaging, University College London, London, United Kingdom*
[4] *Department of Electronic Engineering, NED University of Engineering and Technology, Karachi, Pakistan and*
[5] *Department of Biomedical Engineering, Melbourne School of Engineering, The University of Melbourne, Melbourne, VIC 3010, Australia*
(Dated: March 13, 2019)

Neural information flow is inherently directional. To date, investigation of directional communication in the human structural connectome has been precluded by the inability of non-invasive neuroimaging methods to resolve axonal directionality. Here, we demonstrate that decentralized measures of network communication, applied to the undirected topology and geometry of brain networks, can predict putative directions of large-scale neural signalling. We propose the concept of send-receive communication asymmetry to characterize cortical regions as senders, receivers or neutral, based on differences between their incoming and outgoing communication efficiencies. Our results reveal a send-receive cortical hierarchy that recapitulates established organizational gradients differentiating sensory-motor and multimodal areas. We find that send-receive asymmetries are significantly associated with the directionality of effective connectivity derived from spectral dynamic causal modeling. Finally, using fruit fly, mouse and macaque connectomes, we provide further evidence suggesting that directionality of neural signalling is significantly encoded in the undirected architecture of nervous systems.

## INTRODUCTION

Understanding how the structural substrate of connectomes [1, 2] gives rise to the rich functional dynamics observed in nervous systems is a major goal in neuroscience [3–6]. The description of mechanisms underpinning neuronal signalling and communication is a crucial task in addressing this challenge [7–10].

While information can be directly communicated between anatomically connected elements of a nervous system, polysynaptic communication is needed for structurally unconnected elements. Several candidate models of polysynaptic communication have been proposed and evaluated using graph-theoretic representations of nervous systems [9]. Shortest paths routing is the most ubiquitous model [11–13], which proposes that communication occurs via optimally efficient routes. Efficiency in this context refers to routes that traverse either the fewest number of connections (i.e. fewest number of synapses) or the strongest and most reliable connections. However, the computation of shortest paths mandates global knowledge of network topology, a requirement that is unlikely to be met in biological systems [9, 15]. This has motivated research on decentralized models that capitalize on local knowledge of network properties to facilitate information transfer. Examples include navigation [15–17], spreading dynamics [18, 19], communicability [20–22] and diffusion processes [23–25].

Many decentralized communication models are asymmetric [8, 15, 18, 26]. This means that the efficiency of communication between a pair of nodes can be asymmetric; that is, sending information from region $i$ to region $j$ can be performed more efficiently, from a graph-theoretic standpoint, than sending information from region $j$ to region $i$. We coin the term *send-receive communication asymmetry*, or simply *send-receive asymmetry* to describe this property. In the context of the aforementioned pair of regions, we consider region $i$ to be a putative *sender* and region $j$ as a putative *receiver*. Importantly, communication asymmetries can arise in undirected networks, such as current descriptions of the human structural connectome, where knowledge about the directionality of individual connections is unknown. In undirected networks, communication asymmetries arise from the interaction between the communication model and network topology as well as possibly geometry (Fig. 1). While asymmetric communication models have been investigated in brain networks across various species and scales [8, 15, 18], the directional character of information flow inherent to these models remains largely unexamined [26].

The concept of send-receive communication asymmetry provides opportunities to infer putative directions of neural information flow in the human connectome using traditional *in vivo* diffusion MRI coupled with established fiber tracking methods, which inherently cannot resolve the directionality of white matter fibers. Therefore, investigating decentralized network communication measures may help bridge the gap between our symmetric understanding of human connectome structure and the

* caioseguin@gmail.com

ample evidence for its asymmetric functional dynamics [27–29].

Here, we investigate three asymmetric network communication measures: i) navigation efficiency, ii) diffusion efficiency, and iii) search information. We provide multiple lines of evidence supporting the notion that these measures, applied to undirected brain networks, lead to meaningful patterns of send-receive communication asymmetry. We classify cortical regions and functional subsystems as senders (biased towards the efficiency of outgoing paths), neutral (symmetric communication efficiency) and receivers (biased towards the efficiency of incoming paths). Crucially, we use an independent imaging modality—resting-state functional magnetic resonance imaging (fMRI)—to validate our communication asymmetry findings derived from brain networks mapped with diffusion MRI. Using directed non-human connectomes, we investigated whether the directions of neural signalling inferred from send-receive asymmetries are encoded, to a significant extent, in the undirected topology and geometry of brain networks.

## RESULTS

### Measures of send-receive communication asymmetry

Network communication models describe a propagation strategy that delineates the signalling pathways utilized to transfer information between nodes. In turn, a network communication measure quantifies the ease of communication along the identified pathways from a graph-theoretic standpoint. In this paper, we use the broad term *communication efficiency* to denote the ease of communication quantified by different network communication measures. Efficient communication pathways are generally short, traverse few synapses and comprise strong and reliable connections [30].

We considered three asymmetric network communication measures: i) navigation efficiency, ii) diffusion efficiency and iii) search information. Briefly, navigation efficiency [15] relates to the length of paths identified by navigation or greedy routing [16, 31], with higher values of efficiency indicating faster and more reliable communication between nodes. Diffusion efficiency [24] quantifies how many intermediate regions (synapses), on average, a naive random walker needs to traverse to reach a desired destination region. Finally, search information is related to the probability that a random walker will travel from one region to another via the shortest path between them [8, 32], quantifying the extent to which efficient routes are hidden in the network topology. Further details, including the mathematical formulation of these measures, can be found in *Materials and Methods, Network communication measures*.

Communication asymmetry is introduced by the decentralized character of certain network communication models (Fig. 1). Consider the flow of information from one region, termed the *source node*, to another region, termed the *target node*. If this source-target pair is not directly connected, information must flow via a polysynaptic path that traverses one or more intermediate nodes. Decisions on how signals are propagated through the connectome depend on the local topology around each node. Since source and target nodes occupy potentially different vicinities, communication may happen through distinct paths, and thus with different efficiency, depending on the direction of information flow. In contrast, centralized communication models such as shortest path routing yield symmetric paths in undirected networks.

We use $C \in \mathbb{R}^{N\times N\times K}$ to denote a set of communication matrices for $K$ individuals, where $C(i,j,k)$ denotes the communication efficiency from node $i$ to node $j$ for individual $k$, under an arbitrary communication measure (Fig. 2a). The difference in communication efficiency for opposing directions of information flow between $i$ and $j$ is given by $\Delta(i,j,k) = C(i,j,k) - C(j,i,k)$. We perform a one-sample t-test to determine whether the mean of the distribution $\Delta(i,j,k=1...K)$ is significantly different to 0 (Fig. 2c). This yields a t-statistic, termed $A(i,j)$, which quantifies the extent of communication asymmetry between $i$ and $j$. In particular, if $A(i,j)$ is significant and greater than zero, we conclude that communication can occur more efficiently from node $i$ to node $j$, rather than from node $j$ to node $i$. Note that $A(i,j) = -A(j,i)$, and thus if $A(j,i)$ is significantly less than zero, we reach the same conclusion. Repeating this test independently for all pairs of nodes yields the communication asymmetry matrix $A$, for which values are symmetric about the main diagonal, but with opposite signs.

The above measure is specific to pairs of nodes. We use a variation of this test to compute regional send-receive communication asymmetry by taking into account all outgoing and incoming communication paths of a given node (*Materials and Methods, Communication asymmetry test*). Regions that show a significantly higher efficiency of outgoing (incoming) communication are classified as putative senders (receivers), while nodes that do not favour a direction of information flow are classified as neutral.

### Senders and receivers of the human connectome

Whole-brain white matter tractography was applied to high-resolution diffusion MRI data acquired in $K = 200$ healthy adults (age 21–36, 48.5% female) participating in the Human Connectome Project [33]. Structural brain networks were mapped at several spatial resolutions ($N = 256, 360, 512$ regions; *Materials and Methods, Connectome mapping*). For each individual, the resulting weighted adjacency matrix was thresholded at 10%, 15% and 20% connection density to eliminate potentially spurious connections [34], and subsequent analyses were carried out on the obtained weighted connectomes. Communication matrices quantifying the communication ef-

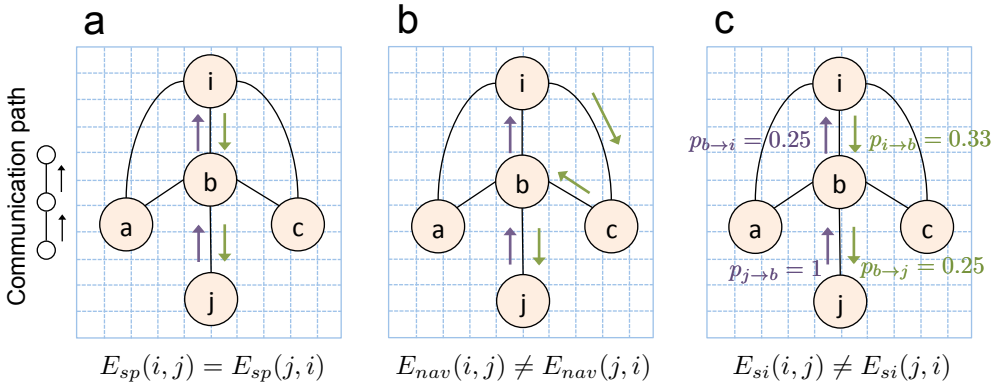


**FIG. 1.** Illustrative examples of send-receive communication asymmetry in a spatially-embedded, unweighted and undirected network. Communication efficiency from node $i$ to $j$ under measure $x \in \{nav, sp, si\}$ is denoted $E_x(i,j)$, where *nav*, *sp* and *si* indicate navigation efficiency, shortest path efficiency and search information, respectively. Shortest path and navigation efficiencies are computed as the inverse of the number of connections comprising shortest and navigation paths, respectively. Search information relates to the probability that a random walker will travel between two nodes via the shortest path linking them. The path identified under each communication model is designated with green ($i \to j$) and mauve ($j \to i$) arrows. Send-receive communication asymmetry refers to $E_x(i,j) \neq E_x(j,i)$. **(a)** Shortest path efficiency is a symmetric communication measure in undirected networks, and thus $E_{sp}(i,j) = E_{sp}(j,i)$. **(b)** Navigation routes information by progressing to the next directly connected node that is closest in distance to the target node. This results in the *i-c-b-j* and *j-b-i* navigation paths, with respective efficiency $E_{nav}(i,j) = 0.33$ and $E_{nav}(j,i) = 0.5$. Hence, navigation is more efficient from node $j$ to node $i$. **(c)** Arrows denote the symmetric shortest paths between $i$ and $j$. Arrows are annotated with the probabilities that a random walker will traverse their respective connections based on node degree (e.g., each of the 3 connections of node $i$ has approximately 0.33 probability to be traversed by a random walker leaving $i$). We have $E_{si}(i,j) \propto 0.33 \times 0.25 = 0.0825$ and $E_{si}(j,i) \propto 1 \times 0.25 = 0.25$. Hence, a random walker has higher probability of travelling via the shortest path in the $j \to i$ direction, characterizing search information asymmetry between $i$ and $j$.

ficiency between every pair of regions were computed (Fig. 2a, *Materials and Methods, Network communication models*) and used to derive measures of send-receive asymmetry in communication efficiency (*Materials and Methods, Communication asymmetry test*). We focus on describing the results for $N = 360$ at 15% connection density. Results for other connection densities and parcellation resolutions can be found in *Supplementary Information*.

Significant asymmetries in the efficiency of sending versus receiving information were evident for most cortical regions (Fig. 3a,d,g). Regional values of send-receive asymmetry were significantly correlated across regions among the communication measures investigated (navigation and diffusion: $r = 0.29$, navigation and search information: $r = 0.31$, diffusion and search information: $r = 0.85$; all $P < 10^{-7}$). Based on these send-receive asymmetries, we classified all regions as senders, receivers or neutral. As expected from the strong correlation between them, diffusion and search information asymmetries led to similar classifications, likely due to their mutual dependence on random walk processes. While communication under navigation is guided by different mechanisms, classification consistency across measures was greater than expected by chance (*Supplementary Information, Note 1*).

Primary sensory and motor regions were identified as senders (A1, S1 and M1 across all communication measures and V1 for navigation and diffusion). This is consistent with the notion that early auditory, visual and sensory-motor areas constitute the three main input streams to the cortex, being the first to process sensory stimuli that are subsequently transmitted to association regions [35, 36]. In contrast, expanses of the orbital and polar frontal cortices, the medial and dorsolateral prefrontal cortices, and the precuneus were classified as receivers. These regions have been proposed as putative functional hubs, supporting abstract and high-order cognitive processes by integrating multiple modalities of information [37–39]. Other regions consistently identified as senders included portions of the superior temporal, medial temporal and posterior cingulate cortices, while parts of the MT+ complex, intraparietal sulcus cortex, and dorsal and ventral streams consistently ranked amongst receivers. Certain regions were classified as senders under one communication measure but receivers under another measure, possibly reflecting how the three communication measures uniquely interact with connectome topology. Inconsistently classified regions included portions of the paracentral, cingulate, middle temporal and inferior temporal cortices. Details on how to access complete send-receive asymmetry tables and cortical maps are provided in *Materials and methods, Data and code availability*.

Despite significant asymmetries in the efficiency of sending versus receiving information *within* individual re-

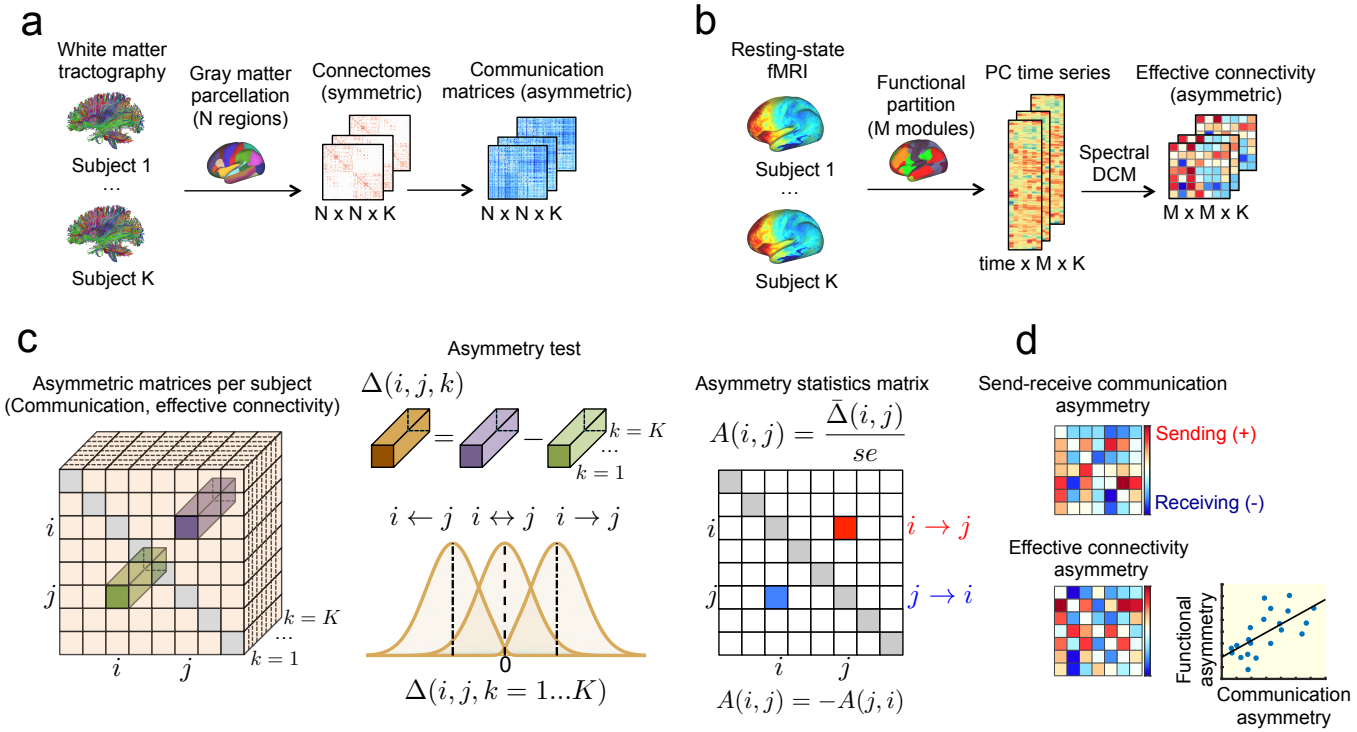


**FIG. 2.** Methodology overview. **(a)** White matter tractography applied to diffusion MRI data for $K = 200$ adults participating in the HCP was used to map undirected (i.e., symmetric) weighted adjacency matrices representing the structural connectivity between $N = 256, 350, 512$ cortical regions. Navigation efficiency, diffusion efficiency and search information were computed between every pair of regions to generate asymmetric communication matrices. **(b)** Resting-state fMRI data for the same HCP participants was used to compute principal component (PC) time series summarizing the functional activity of $M = 7, 17, 22$ cortical subsystems. For each individual, effective connectivity between cortical subsystems was computed using spectral DCM. **(c)** Schematic of the communication asymmetry test. First, for a pair of nodes $i$ and $j$, the difference in communication efficiency between the $i \rightarrow j$ and $j \leftarrow i$ directions was computed. Performing this for $K$ individuals yielded the distribution $\Delta(i, j, k = 1...K)$. Communication asymmetry was assessed by performing a one-sample t-test to determine whether the mean of this distribution is significantly different to 0, with $A(i, j)$ defined as the resulting matrix of t-statistics. **(d)** The asymmetry test was applied to compute $M \times M$ matrices of communication and effective connectivity send-receive asymmetries between modules. We sought to test for correlations across the corresponding elements of these two matrices.

gions, these send-receive asymmetries were superposed atop a strong correlation *across* regions between send and receive efficiency (navigation: $r = 0.95$, search information: $r = 0.79$; both $P < 10^{-15}$; Fig. 3b,e). In other words, efficient senders were also typically efficient receivers, and vice versa. Therefore, while all senders were by definition significantly more efficient at sending than receiving, some senders were in fact *less* efficient at sending than some receivers. In contrast, send and receive efficiencies were not correlated under diffusion ($r = -0.1, P = 0.1$). In addition, send efficiency was relatively uniform across regions under diffusion, while receive efficiency showed markedly higher regional diversity. This result is in line with previous observations of the importance of local connectivity around target nodes for diffusive communication processes [26].

Node degree was anti-correlated with send-receive asymmetries under diffusion and search information ($r = -0.54, -0.70$, respectively, both $P < 10^{-15}$), with low- and high-degree regions more likely to be senders and receivers, respectively. This was not the case for navigation ($P = 0.48$), where senders and receivers were uniformly distributed across the degree distribution. This suggests that diffusive communication is considerably influenced by node degree, while other topological and geometric network properties shape send-receive asymmetries under navigation.

### Senders and receivers situated within cortical gradients

Next, we aimed to investigate whether senders and receivers would reside at opposing ends of previously delineated whole-brain gradients of functional connectivity [40]. We focussed on the uni- to multimodal cortical gradient mapped by Marguiles and colleagues [38]. Under all three communication measures, senders were

more likely to be located at the unimodal end of the gradient, whereas the multimodal end was occupied by receivers. More specifically, send-receive asymmetry and cortical gradient eigenvalues were significantly correlated across regions (navigation: $r = -0.20$, search information: $r = -0.29$, diffusion: $r = -0.30$, all $P < 10^{-4}$). In further analyses, regions were classified as unimodal (U), transitional (T) or multimodal (M) based only on the cortical gradient (*Materials and Methods, Cortical gradient of functional heterogeneity*). The median send-receive asymmetry across unimodal and transitional areas was significantly increased in comparison to multimodal regions (Fig. 3c,f,i; Wilcoxon rank sum test $P_{T>M} = 0.01$, $2 \times 10^{-4}$, $2 \times 10^{-4}$ and $P_{U>M} = 4 \times 10^{-4}$, $3 \times 10^{-6}$, $8 \times 10^{-7}$, for navigation, search information and diffusion, respectively). Send-receive asymmetry did not differ between unimodal and transitional regions.

These results were generally robust to variations in cortical parcellation and connection density thresholds (Fig. S1 and S2). Taken together, our findings demonstrate that decentralized communication measures applied to the undirected human connectome unveil regional distinctions between putative senders and receivers. Furthermore, we show that knowledge about the direction of information flow can elucidate novel organizational structure within established cortical hierarchies, such as the biases towards outgoing and incoming communication efficiency of uni- and multimodal regions, respectively.

### Senders and receivers of cortical subsystems

Having characterized senders and receivers at the scale of areal regions, we next sought to investigate send-receive asymmetries between large-scale cortical subsystems. We assigned cortical regions to distributed cognitive systems according to established resting-state networks comprising $M = 7$ and 17 subsystems (Fig. S3a,b) [41]. In addition, we employed a multimodal partition of the cortex into $M = 22$ spatially contiguous subsystems (Fig. S3c) [36]. Regional communication matrices were downsampled to subsystem resolution and send-receive asymmetries were computed for each pair of subsystems (*Materials and Methods, Cortical subsystems*).

In keeping with the regional findings, we found that some subsystems were putative senders while others were predominantly receivers. Send-receive asymmetry matrix values were significantly correlated across subsystems among the communication measures investigated (e.g., navigation and diffusion: $r = 0.60$, navigation and search information: $r = 0.66$, diffusion and search information: $r = 0.96$; all $P < 10^{-15}$, $M = 17$). Our findings at the subsystem scale were generally consistent across communication measures, and thus we focus on navigation in this section (Fig. 4). Complete results for navigation, diffusion and search information are shown, respectively, in Figs. S4, S5, S6.

As shown in Fig. 4a,b, the somatomotor and ventral attention networks were the most prominent senders for the $M = 7$ partition. Prominent receivers included the default mode, frontoparietal and limbic networks, which were more efficiently navigated from a number of cognitive systems than vice versa. Interestingly, adopting a higher resolution functional partition ($M = 17$) suggested that sub-components of coarse ($M = 7$) resting-state networks can assume different roles as senders and receivers. For instance, the visual network was segregated into early (e.g., V1 and V2) from late areas of the visual cortex (e.g., MT+ complex and dorsal and ventral streams), with the first being a sender and the latter a receiver (Fig. S4). Other systems that exhibited this behaviour included the ventral attention, limbic, somatomotor and default mode networks. These findings reiterate that, despite the presence of asymmetries in send-receive efficiency, cognitive systems are not exclusively senders or receivers, suggesting connectome topology may allow for context-dependent directionality of neural information flow between functional networks.

Finally, we identified senders and receivers for a high-resolution cortical partition comprising $M = 22$ subsystem [36]. This enabled a fine-grained, yet visually interpretable, characterization of send-receive asymmetries (Fig. 4c). For instance, navigation paths were more efficient departing from V1 (subsystem 1) towards the early visual cortex and MT+ complex (subsystems 2 and 5), the mid cingulate cortex and premotor cortices (subsystem 7 and 8), different regions of the parietal cortex (subsystems 16 to 18), and areas in the frontal and prefrontal cortices (subsystem 19 to 22). Meanwhile, navigation paths were more efficient departing from the ventral system (subsystems 4), early and association auditory cortices (subsystem 10 and 11) and the temporal cortex (subsystem 13 and 14) towards V1.

More generally, across all three measures, the identification of senders and receivers was consistent between regional and subsystem scales. Cortical domains associated with auditory, somatosensory and motor processes ranked amongst the strongest senders, while frontal and prefrontal areas consistently featured amongst the most prominent receivers (Figs. S4, S5 and S6). Together, these results provide putative multi-scale maps of how the structural substrate of the human connectome may facilitate directional information flow between cognitive subsystems.

### Senders, receivers and effective connectivity

We sought to validate our characterization of subsystems as senders or receivers using an independent data modality. To this end, time series summarizing the functional dynamics of cortical subsystems were extracted from resting-state functional MRI data for the same $K = 200$ HCP participants. For each individual, we used spectral DCM [42, 43] to compute effective connectivity between cortical subsystems ($M = 7, 17, 22$, see

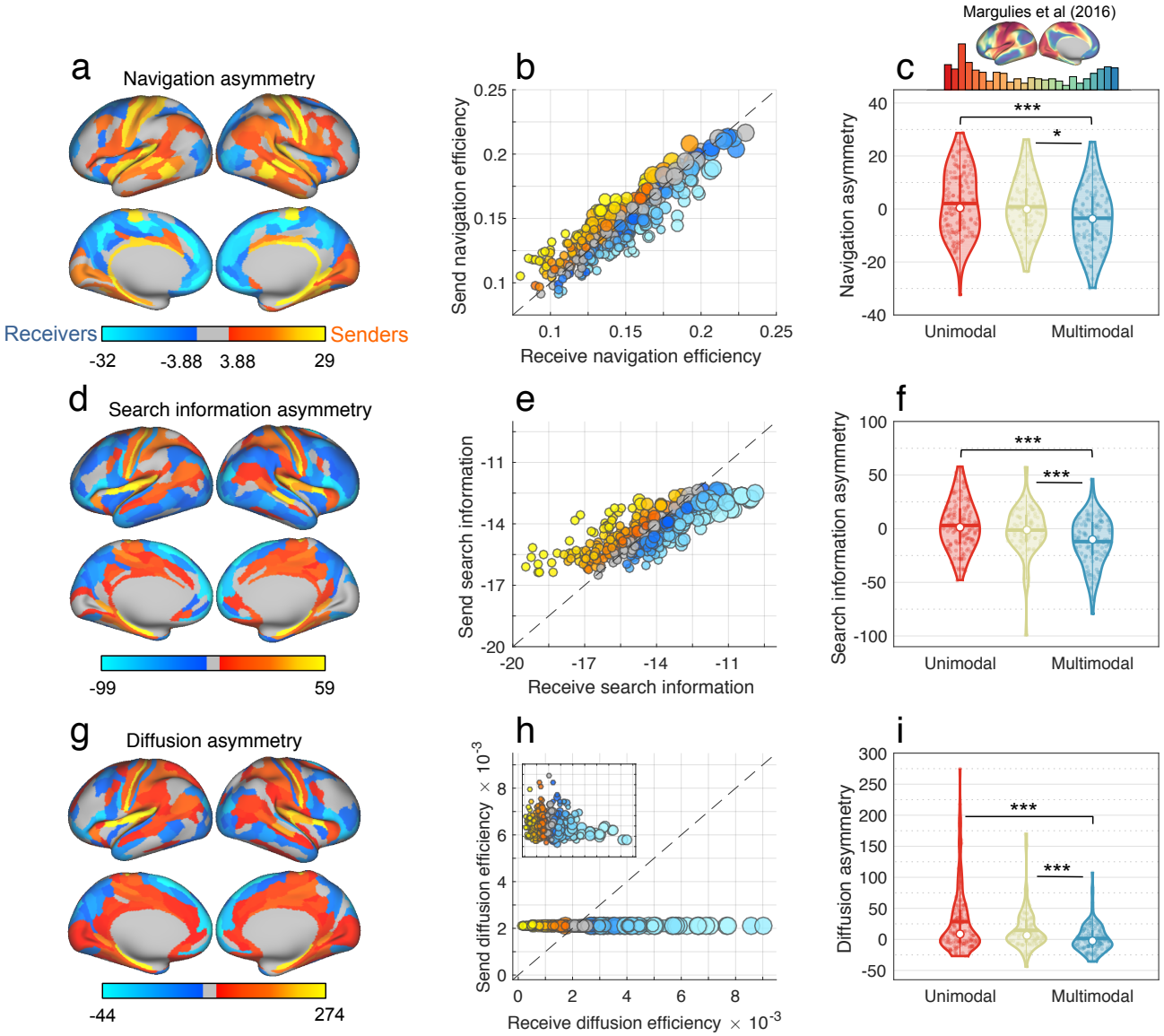


**FIG. 3.** Send-receive communication asymmetry in the human connectome ($N = 360$ at 15% connection density). **(a)** Putative senders (orange) and receivers (blue) under navigation projected onto the cortical surface. Regions colored gray are neutral and do not show significant send-receive asymmetry. **(b)** Scatter plot showing correlation between send and receive efficiency across regions under navigation. Send and receive efficiency values were aggregated across all individuals for each region. Markers are colored according to send-receive asymmetry values (colors approximately match that of panel a). Small, medium and large markers represent nodes with low ($\kappa < 50$), medium ($50 \leq \kappa \leq 100$) and high ($\kappa > 100$) degree, respectively. The dashed line marks the $x = y$ identity line. The distance between markers and the identity line provides a geometric interpretation of regional bias towards sending ($x < y$) or receiving ($x > y$) efficiencies. **(c)** Top: Distribution of the cortical gradient eigenvalues used as a measure of functional heterogeneity [38]. Bottom: Violin plots showing distribution of send-receive asymmetries for regions classified as unimodal (red), transitional, (beige) and multimodal (blue) regions. Horizontal bars and white circles denote, respectively, the mean and median of the distributions. Stars denote significant differences in between-group medians given by a two-sided Wilcoxon rank sum test (one, two and three stars denote $P < 0.05, 0.005, 0.0005$, respectively). **(d-e)** Search information equivalent of a-c. **(g-i)** Diffusion efficiency equivalent of a-c.

*Materials and Methods, Effective connectivity*). Pairwise effective connectivity asymmetry was computed at the scale of subsystems by applying the previously described asymmetry test to the estimated effective connectivity matrices (Fig. 2c). Importantly, effective connectivity is an inherently directed (asymmetric) measure of connectivity. This allowed us to test whether send-receive asymmetries in communication efficiency (derived from

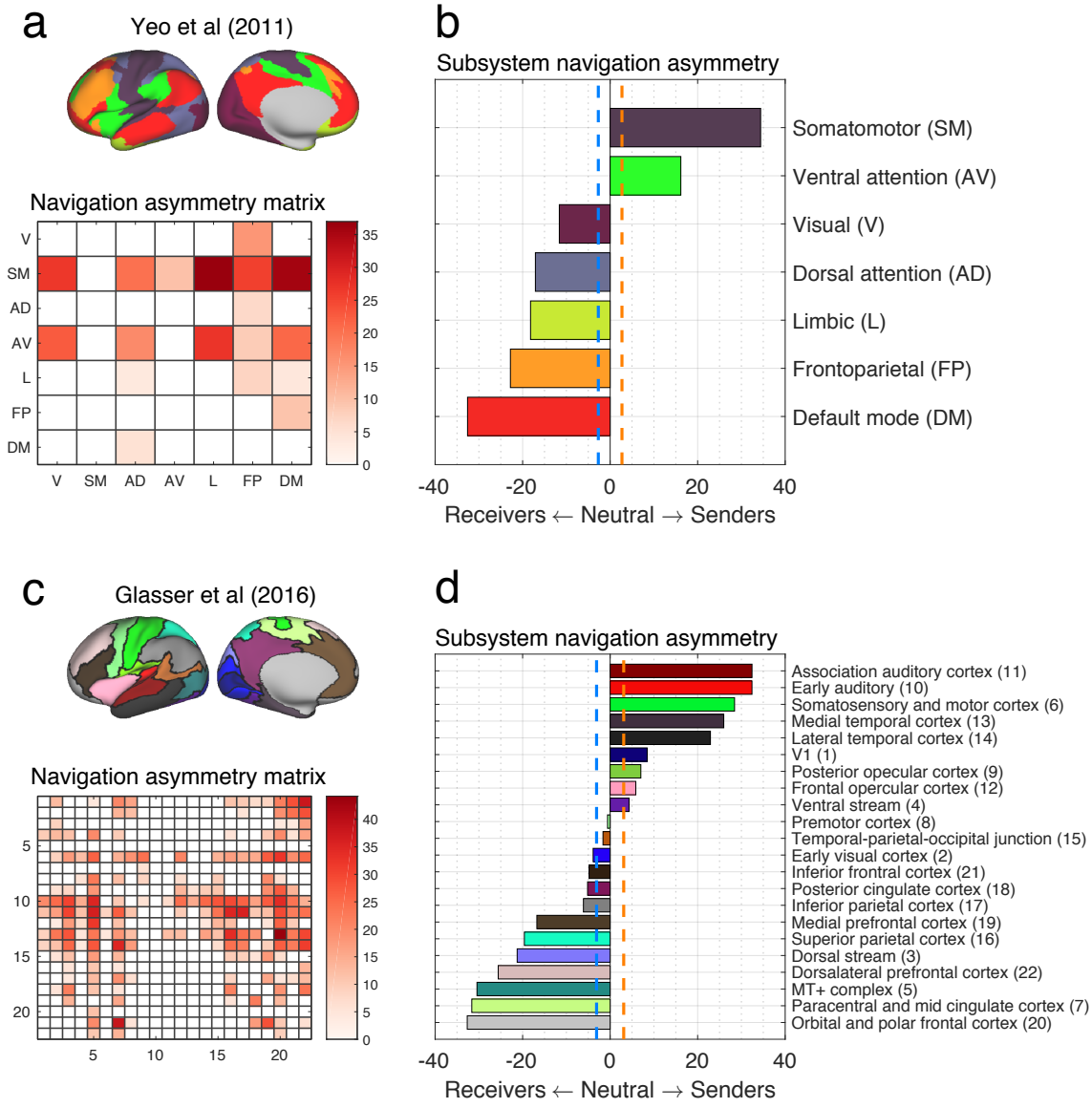


**FIG. 4.** Send-receive asymmetry of cortical subsystems under navigation ($N = 360$ at 15% connection density). **(a)** Projection of $M = 7$ distributed resting-state networks onto the cortical surface (top) and send-receive asymmetry matrix under navigation (bottom). A matrix element $A(i, j) > 0$ denotes that communication occurs more efficiently from $i$ to $j$ than from $j$ to $i$. Send-receive asymmetry values that did not survive multiple comparison correction were suppressed and appear as white cells. For ease of visualization and without loss of information (since $A(i, j) = -A(j, i)$), negative values were omitted. **(b)** Resting-state networks ranked by propensity to send (top) or receive (bottom) information. Dashed vertical lines indicate a significant bias towards outgoing (orange) and incoming (blue) communication efficiency. **(c-d)** Same as (a-b), but for $M = 22$ spatially contiguous cortical subsystems. Numbers listed next to module names identify corresponding rows and columns in the asymmetry matrix.

diffusion MRI) and effective connectivity (derived from resting-state fMRI) are correlated (Fig. 2d).

Communication and effective connectivity send-receive asymmetries were significantly correlated across pairs of subsystems (Fig. 5). These associations were significant for all three communication measures and were replicated across two independent resting-state functional MRI sessions and multiple structural connection densities. For instance, for $M = 17$, fMRI session 1 and 15% connection density, we found $r = 0.51, 0.32, 0.32$ for navigation, diffusion and search information, respectively (all $P < 10^{-4}$). Similarly, for $M = 22$, fMRI session 2 and 15% connection density, we obtained $r = 0.45, 0.48, 0.48$ for navigation, diffusion and search information, respectively (all $P < 10^{-12}$). No significant correlations were found for $M = 7$, possibly due to the lack of statisti-

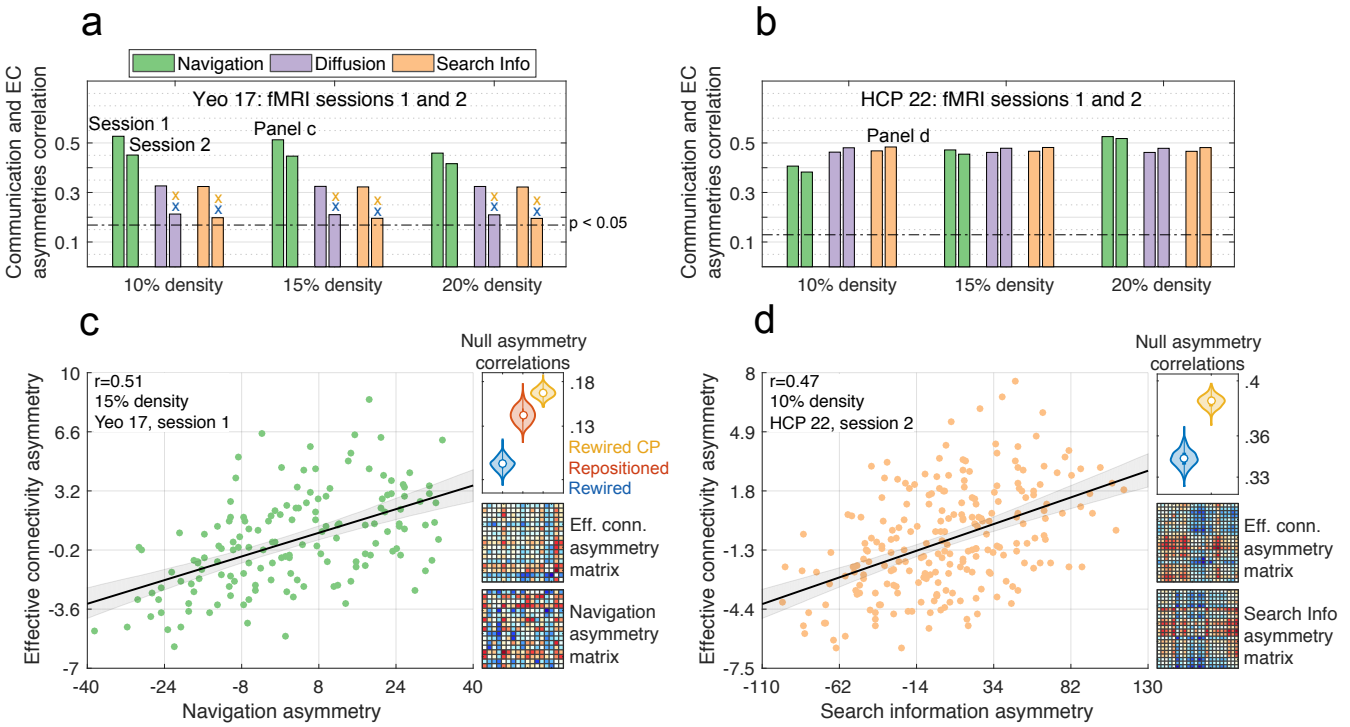


**FIG. 5.** Effective connectivity used to validate send-receive asymmetries arising from network communication in structural connectomes ($N = 360$). **(a)** Correlation across pairs of cortical subsystems ($M = 17$) in send-receive asymmetry values from effective connectivity and three communication measures: i) navigation (green), ii) diffusion (violet), and iii) search information (beige). Correlations were computed for two independent resting-state fMRI sessions (Sessions 1 and 2) and multiple structural connection density thresholds (10, 15 and 20%). Significance threshold of $P < 0.05$ is indicated with a dotted line. Crosses mark associations that were *not* statistically stronger than those found in families of 1000 rewired (blue) and 1000 cost-preserving rewired (yellow) connectomes, respectively (repositioned connectomes, relevant for navigation, led to statistically weaker associations in all scenarios). **(b)** Replication of Panel **a** for a cortical partition comprising $M = 22$ subsystems. **(c)** Left: scatter plot illustrating the correlation between navigation and effective connectivity asymmetries for $M = 17$, 15% connection density and fMRI session 1. Shadows denote the 95% bootstrapped confidence interval. Top-right: Distribution of correlations obtained for families of 1000 rewired (blue), repositioned (red) and cost-preserving rewired (yellow) connectomes. Bottom-right: Send-receive asymmetry matrices for effective connectivity (resting-state functional MRI) and navigation (diffusion MRI). The upper-triangular elements of these two matrices were correlated to test whether senders and receivers were consistently identified across independent modalities. **(d)** Replication of Panel **c** for search information, $M = 22$, 10% connection density and fMRI session 2. EC: effective connectivity; $r$: Pearson correlation coefficient.

cal power afforded by only 21 data points. These results suggest that biases in the directionality of neural signalling inferred from the structural connectome are related to the directions of causal functional modulation during rest. Therefore, they establish a correspondence between structural (connectome topology and network communication measures) and functional (effective) directions of neural information flow.

We sought to determine whether the above association between communication and effective connectivity could be explained by certain properties of connectome organization. We generated ensembles of randomized connectomes in which (i) connectome topology was rewired while preserving degree distribution [77]; (ii) connectome topology was rewired while preserving degree distribution and total network cost (defined as the sum of Euclidean distances between structurally connected nodes [13]); and (iii) nodes were spatially repositioned while preserving topology (relevant only for navigation; see *Supporting Information, Note 2*). For all families of randomized connectomes, correlations between asymmetries in effective connectivity and communication efficiency were significantly decreased compared to empirical results (e.g., Fig. 5c,d top-right corner, all $P < 10^{-3}$; with the exception of diffusion and search information for the $M = 17$ partition in fMRI session 2, Fig. 5a). These results indicate that the relationship between send-receive asymmetry and directionality of functional modulation cannot be straightforwardly attributed to degree distribution, network cost or a combination of the two, suggesting the importance of more nuanced topological or geometric properties of connectome organization to large-scale neural signalling.

### Senders and receivers in directed non-human connectomes

Invasive connectome reconstruction techniques allow for the resolution of axonal directionality, producing directed connectomes for a host of non-human species [44]. Using directed connectomes of the fruit fly (*drosophila*) [45, 46], mouse [47, 48] and macaque [49] (*Materials and methods, Non-human connectomes*), we aimed to determine the extent to which send-receive asymmetry is determined by axonal fiber directionality and/or the undirected topology of nervous systems. To this end, we first computed send-receive asymmetries for the directed connectomes. In this case, communication asymmetry is introduced both by the asymmetric character of the network communication measures and by the presence of directed connections. Next, we symmetrized the non-human connectomes by removing connection directionality, so that all connections could be traversed bidirectionally (*Materials and methods, Symmetrized non-human connectomes*), and recomputed send-receive asymmetries for the resulting undirected networks. In this scenario, as with human diffusion-derived connectomes, asymmetries are introduced solely by the asymmetry inherent to the network communication measures. We tested whether send-receive asymmetry values computed in the directed (original) and undirected (symmetrized) non-human connectomes were correlated across regions. Evidence of a correlation would suggest that the undirected topology and geometry of connectomes are influential in determining the directionality of neural signalling regardless of axonal fiber orientation.

For the binarized (unweighted) connectomes of all species, undirected diffusion and search information asymmetries were strongly correlated with their directed counterparts (fly: $r = 0.95, 0.96$, mouse: $r = 0.58, 0.50$, macaque: $r = 0.87, 0.75$, for diffusion and search information asymmetries, respectively; all $P < 10^{-10}$; Fig. 6a,c,d). Non-human connectomes are typically characterized by high connection density, a property that is even more accentuated after symmetrizing connections (fly: 83%, 89%, mouse: 53%, 70%, macaque: 66%, 79%, directed (original) and undirected (symmetrized) connection densities, respectively). Binary navigation paths are seldom asymmetric for densely connected networks [15], restricting the comparison between directed and undirected send-receive asymmetries under navigation. Furthermore, in a binary analysis, the relationship between directed and undirected asymmetries may follow trivially from the high connection density of the directed networks, since original and symmetrized topologies will be closely related. Considering connection weights addresses this issue by taking into account the heterogeneous distribution of connectivity strengths of these networks [49]. Across species, send-receive asymmetries of weighted connectomes were also correlated between directed and undirected versions (fly: $r = 0.58, 0.84, 0.41$, mouse: $r = 0.34, 0.32, 0.38$, macaque: $r = 0.67, 0.80, -0.26$, for navigation, diffusion and search information asymmetries, respectively; all $P < 10^{-10}$, with the exception of $P = 0.01$ for weighted search information in the macaque; Fig. 6b,e,f). This suggests that the distinction between putative senders and receivers is not exclusively determined by the directionality of individual fibers, but is rather partially shaped by the undirected topology of nervous systems. Therefore, even in the absence of information about the directionality of all individual connections, we can still estimate the directionality of information flow in brain networks based on their topological and geometrical characteristics.

## DISCUSSION

The present study focused on characterizing the directionality of information flow in human and non-human brain networks. Previous work has explored differences between the communication efficiency of homotopic regions in order to characterize cortical lateralization [14]. In a recent study, Avena-Koenigsberger and colleagues presented a first account of differences between send and receive communication in brain networks [26]. The authors proposed source and target closeness centrality measures to describe incoming and outgoing communication along a decentralized–centralized spectrum of routing models. Our concept of send-receive communication asymmetry builds on these efforts. We contribute a statistical framework to estimate directionality of neural signalling, as well as to identify putative sender and receiver nodes, in connectomes lacking any intrinsic directionality information, such as those mapped with diffusion MRI and tractography.

Our results consolidate the utility of disparities between incoming and outgoing propagation processes inherent to decentralized network communication models. Send-receive communication asymmetry of cortical regions and subsystems recapitulated, from a structural connectivity standpoint, (i) functional heterogeneity gradients and (ii) directions of functional modulation intrinsic to neural fluctuations at rest (effective connectivity). Finally, we found that send-receive asymmetry could still be recovered after suppressing the directionality of all individual connections in directed non-human connectomes. This suggests that the geometry and topology of nervous systems play a crucial role in shaping the direction of information flow.

Importantly, we reiterate that a significant send-receive asymmetry does not preclude information transfer in a particular direction, in the same way that regions classified as senders (receivers) are capable of receiving (sending) information. Indeed, send and receive efficiencies under navigation and search information were positively correlated across regions. Interestingly, we also found that coarse functional networks with significant biases towards incoming or outgoing communication are typically comprised of subcomponents placed along dif-

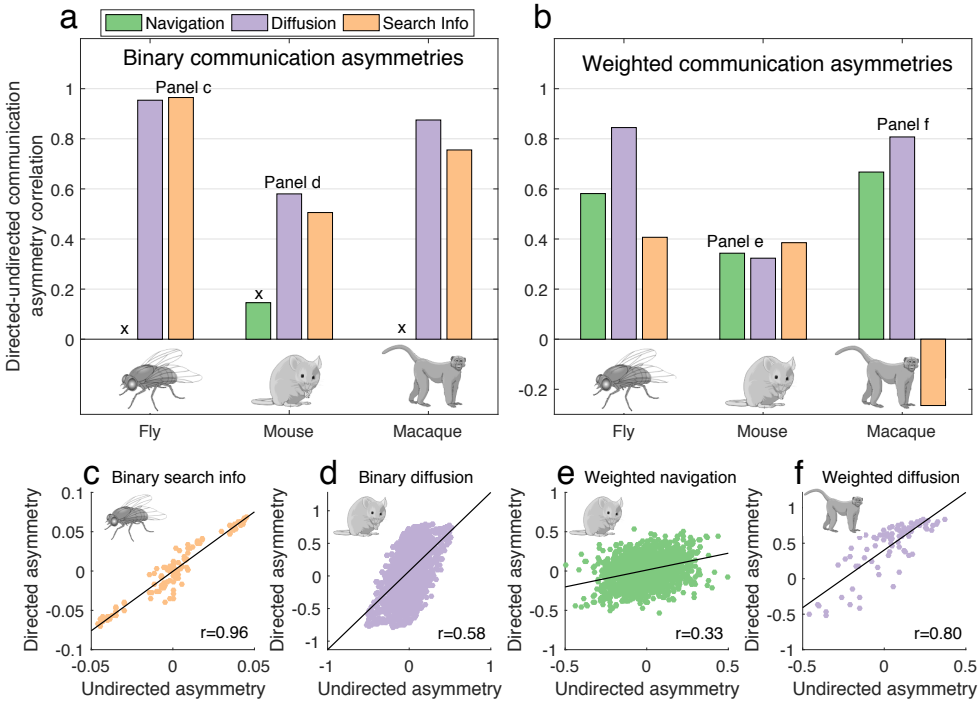


**FIG. 6.** Comparison between directed and undirected (symmetrized) send-receive asymmetries for the connectomes of the fly, mouse and macaque. **(a)** Correlation across regions in send-receive asymmetry values between directed and undirected navigation (green), diffusion (violet) and search information (beige) asymmetries for binarized (unweighted) connectomes. Black crosses indicate *non-significant* ($P > 0.05$) or undefined (in the case of lack of communication asymmetry) correlations. **(b)** Same as (a), but for weighted connectomes. **(c-f)** Scatter plots illustrating the association between directed and undirected communication asymmetries.

ferent positions of the sender-receive spectrum. This may facilitate, for instance, feedback loops in which high-order regions send information to sensory cortices, allowing for flexible and context-dependent transfer of neural information. These results support the notion that cortical computations do not follow a strictly serial paradigm, but rather involve distributed hierarchies of parallel information processing [41, 50].

Navigation efficiency, diffusion efficiency and search information led to similar patterns of send-receive asymmetry despite important conceptual differences in the network communication models associated with these measures. This indicates that our results may be primarily driven by specific properties of brain networks, rather than by aspects particular to one network communication measure. Randomized connectomes generally failed to reproduce the observed relationship between send-receive asymmetries and effective connectivity, suggesting that complex organisational properties of nervous systems are necessary to shape the directionality of neural signalling.

The analysis of non-human directed connectomes contributes further insights into our human connectome results. We found a significant agreement between send-receive asymmetries computed from original directed networks and their symmetrized counterparts. Despite the importance of directed connections to brain network topology [49–51], this finding provides cross-species evidence that the undirected architecture of nervous systems encodes information about signalling directionality. In addition, it further consolidates the utility of studying directional dynamics using undirected networks, suggesting that the putative directions of neural information flow inferred from human connectomes are pertinent despite the lack of directed connections.

Several studies of axonal tract-tracing and non-human connectomes [37, 50, 52], macroscale gradients of cortical organization [38, 40, 53], and computational models of neuronal dynamics [29, 54–57] converge to a common conceptualization of cortical hierarchies. The bottom of the hierarchy tends to comprise high-frequency, low-degree, unimodal, sensory and motor areas that constitute the main inputs of perceptual information to the brain. At the top, low-frequency, high-degree, multimodal regions are conjectured to integrate multiple streams of information in order to support higher cognitive functions. Our observations of a send-receive spectrum of cortical regions and subsystems complements this description of neural organization, placing senders and receivers, respectively, at the uni- and multimodal ends of the hierarchy.

We used spectral DCM applied to resting state fMRI to quantitatively validate the send-receive asymmetries inferred from the structural connectomes mapped with tractography and diffusion MRI. Recent work has demonstrated the validity of spectral DCM in multi-site longitudinal settings [58] and using optogenetics combined with functional MRI in mice [59]. The choice to use spectral DCM over the traditional task-based DCM was motivated by two important factors. First, spectral DCM infers effective connectivity from resting-state fMRI data, allowing validation of our findings independent of hypotheses about the directionality of causal connectivity specific to certain task scenarios. In addition, recent evidence indicates that functional connectivity topology at rest shapes task-evoked fluctuations, highlighting the cognitive relevance of resting-state neural dynamics [60, 61]. Second, spectral DCM is capable of handling relatively large networks comprising many regions [62]. This enabled a direct comparison between asymmetries in send-receive efficiency and effective connectivity at the level of subsystems spanning the whole cerebral cortex. Our results provide cross-modal evidence that network communication measures accurately capture aspects of directional causal influences between neural systems. Future research validating and further exploring this relationship is necessary. For instance, network communication measures may help formulate hypotheses for DCM studies, potentially reducing the number of candidate models based on structurally-derived communication asymmetry [63].

Several limitations of the present study should be considered. Alternative asymmetric network communication measures such as Markovian queuing networks [64], linear transmission models of spreading dynamics [18, 19], cooperative learning [65] and diffusion processes based on memory-biased random walks [23] can lead to further insight into the large-scale directionally of neural signalling. Additional measures of directed functional connectivity such as Granger causality [66] and structural equation modeling [67] may provide supplementary means of cross-modal validation. Tractography algorithms are prone to a number of known biases, potentially influencing results regarding human structural connectomes [34, 68, 69]. Lastly, the human connectomes considered in this study did not include subcortical regions, due to challenges in performing tractography within the subcortex. This limitation should be addressed in future studies, given the important role of subcortical regions in mediating neural signalling between cortical areas.

In conclusion, we showed that the large-scale directionality of neural signalling can be inferred, to a significant extent, from the interaction between decentralized network communication measures and the undirected topology and geometry of brain networks. These results challenge the belief that connectomes mapped from *in vivo* diffusion data are unable to characterize asymmetric interactions between cortical elements. Our findings introduce decentralized network communication models as a new avenue to explore directional functional dynamics in human and non-human connectomes.

## MATERIALS AND METHODS

### Connectivity data

#### *Human connectomes*

Minimally preprocessed diffusion-weighted MRI data from 200 healthy adults (age 21–36, 48.5% female) was obtained from the Human Connectome Project (HCP) [33]. Details about the acquisition and preprocessing of this diffusion MRI are described in [70, 71].

Connectome analyses are sensitive to the number of nodes used to reconstruct brain networks [72]. We aimed to reproduce our key findings for human connectomes constructed with different granularities of cortical segmentation comprising $N = 256, 360, 512$ regions/nodes. The parcellations for $N = 256, 512$ segment the cortex into approximately evenly sized regions that respect predefined anatomical boundaries. Details on the construction of these parcellations are described in [15]. In addition, we mapped connectomes using the HCP MMP1.0 atlas ($N = 360$), a multi-modal cortical parcellation based on the combination of structural, diffusion and functional imaging data from the HCP [36].

Diffusion tensor imaging combined with a deterministic tractography pipeline was used to map connectomes for each individual. Deterministic tractography leads to less false positive connections than other reconstruction methods, and thus may better suit connectome mapping compared to alternative tractography methods [34, 68, 69]. Computations were carried out using MRtrix3 [73] with the following parameters: FACT tracking algorithm, $5 \times 10^6$ streamlines, 0.5 mm tracking step-size, 400 mm maximum streamline length and 0.1 FA cutoff for termination of tracks. Connection strength between a pair of regions was determined as the number of streamlines with extremities located in the regions divided by the product of the surface area of the region pair, resulting in a $N \times N$ weighted connectivity matrix per subject. All human connectome analyses were carried out on weighted networks.

#### *Non-human connectomes*

The fruit fly connectome was mapped using images of 12,995 projection neurons in the female *drosophila* brain available in the FlyCircuit database [45, 46]. Single neurons were labeled with green fluorescent protein and traced from whole brain three-dimensional images. Individual neurons were grouped into 49 local processing units with specific morphology and function. The resulting connectome is a $49 \times 49$ weighted, directed, whole-

brain network for the fruit fly, with 83% connection density.

The Allen Institute for Brain Science mapped the mesoscale topology of the mouse nervous system by means of anterograde axonal injections of a viral tracer [47]. Using two-photon tomography, they identified axonal projections from the 469 injections sites to 295 target regions. Building on these efforts, Rubinov and colleagues constructed a directed, bilaterally symmetric, whole-brain network for the mouse, comprising $N = 112$ cortical and subcortical regions with 53% connection density [48]. Connections represent interregional axonal projections and their weights were determined as the proportion of tracer density found in target and injected regions.

Markov and colleagues applied 1615 retrograde tracer injections to 29 of the 91 areas of the macaque cerebral cortex, spanning occipital, temporal, parietal, frontal, prefrontal and limbic regions [49, 74]. This resulted in a $29 \times 29$ weighted, directed, interregional sub-network of the macaque cortico-cortical connections with 66% connection density. Connection weights were estimated based on the number of neurons labelled by the tracer found in source and target regions, relative to the amount found in whole brain.

## Network communication measures

A weighted connectome can be expressed as a matrix $W \in \mathbb{R}^{N\times N}$, where $W_{ij}$ is the connection weight between nodes $i$ and $j$. Connection weights are a measure of similarity or affinity, denoting the strength of the relationship between two nodes (e.g., streamline counts in tractography or fraction of labelled neurons in tract tracing). The computation of communication path lengths mandates a remapping of connection weights into lengths, where connection lengths are a measure of the signalling cost between two nodes [30]. The transformation $L = -\log_{10}(W/(max(W) + min(W_{>0}))$ ensures a monotonic weight-to-length remapping that attenuates extreme weights [8, 75], where $min(W_{>0})$ denotes the smallest positive value in W, preventing the remapping of the maximum value of $W$ to 0.

### *Navigation efficiency*

Navigation (also referred to as greedy routing) is a decentralized network communication model that utilizes information about the network's spatial embedding to route signals without global knowledge of network topology [31]. Navigation is reported to achieve near-optimal communication efficiency in a range of real-world complex networks, including the connectomes of several species [15–17].

Navigation from node $i$ to $j$ was implemented as follows. Progress to $i$'s neighbour that is closest in distance to $j$. Repeat this process for each new node until $j$ is reached—constituting a successful navigation path—or a node is revisited—constituting a failed navigation path. The distance between two nodes was computed as the Euclidean distance between the centroids of their respective gray matter regions.

Let $\Lambda$ denote the matrix of navigation path lengths. If node $i$ cannot navigate to node $j$, $\Lambda_{ij} = \infty$. Otherwise, $\Lambda_{ij} = L_{iu} + ... + L_{vj}$, where $\{u, ..., v\}$ is the sequence of nodes visited during navigation. Navigation efficiency is given by $E_{nav}(i, j) = 1/\Lambda_{ij}$, where $E_{nav}(i, j)$ is the efficiency of the navigation path from node $i$ to $j$ [15].

### *Diffusion Efficiency*

A diffusion process is a network communication model whereby information is broadcast along multiple paths simultaneously [23]. Diffusion can be understood in terms of agents, often termed random walkers, which are initiated from a given region and traverse the network independent of each other by randomly selecting a connection to follow out from each successive region that is visited. Diffusive communication does not mandate assumptions on global knowledge of network topology, constituting, from this perspective, a biologically plausible model for neural communication [9]. Diffusion efficiency [24] is related to how many intermediate regions (synapses), on average, a naive random walker needs to traverse to reach a desired destination region.

Let $T$ denote the transition probability matrix of a Markov chain process with states corresponding to nodes in the adjacency matrix $W$. The probability of a random walker at node $i$ stepping to node $j$ is given by $T_{ij} = W_{ij}/\sum_{n=1}^{N} W_{in}$. The expected number of hops $\langle H_{ij}\rangle$ a random walker takes to travel from node $i$ to node $j$ is given by [76]:

$$\langle H_{ij}\rangle = \sum_{h=0}^{\infty} hP(H_{ij} = h) = \sum_{h=0}^{\infty} P(H_{ij} > h).$$

The probability of a walker requiring more than $h$ hops to reach node $j$ is equal to the sum of the probabilities of the walker being at any node other than $j$ after exactly $j$ hops. To compute this, we define $T_j$ as the matrix $T$ with all elements in the $j$th column set to zero, so that it is impossible for a walker to arrive at node $j$. This way, we have $P(H_{ij} > h) = \sum_{n=1}^{N} \left[T_j^h\right]_{in}$, where $\left[T_j^h\right]_{in}$ expresses the probabilities of walkers departing from $i$ and reaching any other node expect $j$ in exactly $h$ hops. It follows that

$$\langle H_{ij}\rangle = \sum_{h=0}^{\infty}\sum_{n=1}^{N} \left[T_j^h\right]_{in} = \sum_{n=1}^{N} \left[(\mathbb{1} - T_j)^{-1}\right]_{in}.$$

The diffusion efficiency communication matrix is given by $E_{dif}(i, j) = 1/H_{ij}$, where $E_{dif}(i, j)$ quantifies the ef-

ficiency of information flow from node $i$ to node $j$ under a diffusive process [24].

*Search Information*

Search information relates to the probability that a random walker will serendipitously travel between two nodes via their shortest path [32], quantifying the extent to which efficient routes are hidden in the network topology. Previous studies suggest node pairs with an accessible shortest path—characterized by low search information—tend to show stronger resting-state functional connectivity [8].

The connection length matrix $L$ can be used to compute $\Omega$, where $\Omega_{ij} = \{u, ..., v\}$ denotes the sequence of nodes traversed along the shortest path from node $i$ to node $j$. The search information from $i$ to $j$ is given by $SI_{ij} = -log_2(P(\Omega_{ij}))$, where $P(\Omega_{ij}) = T_{iu} + ... + T_{vj}$ and $T$ is the transition probability matrix. We define communication efficiency under search information as $E_{si}(i,j) = -SI_{i,j}$. This way, $E_{si}(i,j)$ quantifies the accessibility of the $\Omega_{ij}$ shortest path under diffusive communication.

**Send-receive communication asymmetry measures**

Send-receive communication asymmetry matrices $A \in \mathbb{R}^{N\times N}$ were computed as detailed in *Measures of send-receive communication asymmetry*. For each pair of regions or subsystems, a one-sample t-test was used to assess whether the mean of the send-receive asymmetry values across all individuals was significantly different from 0. Bonferroni correction was then performed to control for the $N(N-1)/2$ multiple comparisons corresponding to distinct pairs of regions. This was repeated for each of the three communication measures.

The communication asymmetry matrix $A$ refers to pairwise asymmetric interactions between regions. We performed a similar test to derive a regional (i.e., nodewise) measure of send-receive asymmetry. Let $\{S, R\} \in \mathbb{R}^{N\times K}$ denote, respectively, the average send and receive efficiencies of nodes in the network such that $S(i,k) = 1/N \sum_{j=1}^{N} C(i,j,k)$ and $R(j,k) = 1/N \sum_{i=1}^{N} C(i,j,k)$. The difference between outgoing and incoming communication efficiencies of node $i$ is given by $\delta(i,k) = S(i,k) - R(i,k)$. Analogous to the pairwise asymmetry test, we performed a one-sample t-test to determine whether the mean of the distribution $\delta(i, k = 1...K)$ is significantly different to 0. The resultant t-statistic, termed $a(i)$, quantifies the communication asymmetry of node $i$ by taking into account all of its incoming and outgoing communication efficiencies. Nodes with significant and positive (negative) $a$ were classified as senders (receivers), while non-significant values of $a$ were characterized neutral nodes. For each network communication measure, Bonferroni correction was performed to control for multiple comparisons across the $N$ regions.

Regionally-aggregated send and receive efficiencies depicted in the scatter plots of Fig. 3e,h were computed as $s(i) = 1/K \sum_{k=1}^{K} S(i,k)$ and $r(j) = 1/K \sum_{k=1}^{K} R(j,k)$, respectively. For navigation (Fig. 3b), we display the median send and receive efficiencies in order to attenuate outlier efficiency values and aid visualization.

Non-human directed connectomes were constructed from the results of numerous invasive experiments, often combining experiments across multiple animals of a given species to yield a single, representative connectome. As a result, non-human brain networks were not available for multiple individuals, precluding use of the communication asymmetry test defined for human connectomes. As an alternative, for non-human brain networks, we computed the communication asymmetry between nodes $i$ and $j$ as $A(i,j) = (E(i,j) - E(j,i))/(E(i,j) + E(j,i))$, where $E$ is a communication efficiency matrix. While this measure does not constitute a statistical test of communication asymmetry, it allows us to evaluate differences in the directionality of information flow of non-human nervous systems.

**Cortical gradient of functional heterogeneity**

Margulies and colleagues applied a diffusion embedding algorithm to resting-state fMRI data to identify latent components describing maximum variance in cortical functional connectivity [38]. The obtained components, termed "gradients", are conjectured to describe macroscale principles of cortical organization [40]. In particular, the resultant principal gradient ($G_1$) separated uni- from multimodal regions, spanning a spectrum from primary sensory-motor areas on one end, to the regions comprising the default-mode network on the other. We used this gradient as a quantitative measure of cortical functional heterogeneity and compared it to regional send-receive communication asymmetries. To this end, we downsampled the gradient from vertex to regional resolution by averaging the values comprising each of the $N = 256, 360, 512$ cortical areas defined by the parcellations that we used. Regions were grouped into the unimodal ($G_1 \leq -2$), transitional ($-2 < G_1 < 2$) and multimodal ($G_1 \geq 2$) groups shown in Fig. 3.

**Cortical subsystems**

Yeo and colleagues proposed a widely-used partition of the cortical surface into 7 and 17 resting-state functional networks [41]. These networks constitute distributed (i.e., non-contiguous) functional communities that have been implicated in a wide range of cognitive demands, as well as in rest. Glasser and colleagues used multimodal HCP data to identify 360 cortical regions. Subsequently, they grouped these regions into 22 contiguous subsystems

based on geographic proximity and functional similarities [36]. We use these definitions of cortical partitions to investigate send-receive communication asymmetry at the level of subsystems.

First, we transformed the Yeo partitions ($M = 7, 17$) from vertex to regional resolution. This was achieved by assigning each of $N = 360$ cortical regions to the resting-state network with the largest vertex count within the vertices comprising the region. The HCP partition ($M = 22$) does not necessitate this step, since it is already defined in terms of the $N = 360$ of the Glasser atlas.

Second, we downsampled individual communication efficiency matrices from regional ($N = 360$) to subsystem resolution ($M = 7, 17, 22$) by averaging the pairwise efficiency of nodes assigned to the same subsystem. For two subsystems $u$ and $v$, we have

$$E'_{uv} = \frac{1}{|M_u||M_v|} \sum_{\substack{i \in M_u \\ j \in M_v}} E_{ij}$$

where $M_u$ and $|M_u|$ denote, respectively, the set and number of regions belonging to subsystem $u$, $E \in \mathbb{R}^{N \times N}$, and $E' \in \mathbb{R}^{M \times M}$. Across $K$ subjects, this results in a set of communication matrices $C \in \mathbb{R}^{M \times M \times K}$ that is used to compute between-subsystems send-receive communication asymmetries as described in Fig. 2 and *Materials and Methods, Communication asymmetry test.*

The send-receive communication asymmetry for individual cortical subsystems was computed analogous to regional communication asymmetries as described in *Send-receive communication asymmetry measures.* For each network communication measure, Bonferroni correction for $M$ and $M(M-1)/2$ multiple comparisons was applied to individual and pairwise subsystems asymmetries, respectively.

### Send-receive effective connectivity asymmetry

Spectral DCM estimates effective connectivity from resting-state fMRI data. It receives as input time series characterizing the functional dynamics of neural activity and a network model describing how these elements are coupled. As opposed to the more common task-based DCM, spectral DCM estimates effective connectivity in the absence of experimental or exogenous inputs, characterizing functional modulations between neural elements based on intrinsic neural fluctuations at rest. Details on the generative models inherent to spectral DCM as well as the frequency-domain model inversion are described in [42, 62].

Minimally preprocessed resting-state fMRI data for the same $K = 200$ subjects was acquired from the HCP. Functional volumes were acquired during 14m33s at 720 TR, resulting in 1,200 time points. Data from two separate sessions (right-to-left and left-to-right encoding, performed on different days) was used to compute two estimates of effective connectivity for each subject. HCP acquisition and preprocessing of resting-state fMRI are detailed in [70, 71].

We computed the blood-oxygenation-level-dependent (BOLD) signal of $N = 360$ regions by averaging the time series of all cortical surface vertices comprised into a region. Next, the $N$ regions were partitioned into $M$ cortical subsystems as described in *Materials and Methods, Cortical subsystems.* For each subsystem, we performed a principal component analysis on all the time series belonging to it. The resultant first principal component was used to summarize the functional activity of a subsystem in a single time series. The $M \times 1,200$ time series of principal components were used as input to spectral DCM, together with a fully connected model of coupling strengths ($\mathbb{1}_{M \times M}$), enabling estimation of effective connectivity between subsystems covering the whole cortex [62]. Spectral DCM estimations were carried out using SPM12.

Spectral DCM estimates signed effective connectivity, with positive and negative values indicating excitatory and inhibitory influences, respectively. Under the assumption that both excitatory and inhibitory processes are facilitated by communication between neural elements, we considered the absolute value of the estimated coupling strengths.

The obtained coupling strengths of each subject were concatenated. For each resting-state session, this yielded a $M \times M \times K$ effective connectivity matrix, which were used to compute effective connectivity asymmetry between cortical subsystems, as described in Fig. 2 and *Materials and Methods, Communication asymmetry test.*

### Symmetrized non-human connectomes

Directed non-human connectomes ($W_d$) were symmetrized in order to omit information on axonal directionality. Undirected (symmetric) networks ($W_u$) were computed as $W_u = (W_d + W_d^T)/2$, ensuring that all original connections in $W_d$ can be traversed bidirectionally in $W_u$. Directly connected node pairs do not show send-receive asymmetry under navigation, since both directions of routing will necessarily occur via the single connection linking the two nodes. For this reason, we restricted the analyses in *Senders and receivers in non-human connectomes* to node pairs that did not share a direct structural connection in $W_u$.

### Data and code availability

All analyses in the present study were carried out on publicly available datasets. Structural and effective human brain networks were mapped from Human Connectome Project data [33] (`https://db.humanconnectome.org/`). The fruit fly connectome was collated from data available in `http://www.flycircuit.tw` and can be found in the supplementary information of reference

[46]. The macaque connectome was derived from data available at `http://core-nets.org/` [49]. The mouse connectome was constructed from resources provided by the Allen Institute for Brain Science (`https://mouse.brain-map.org/` [47]) and is available in the supplementary information of reference [48]. The cortical gradient of functional connectivity from reference [38] is available at `https://www.neuroconnlab.org/data/index.html`.

Send-receive communication asymmetry measures and other data necessary to generate key figures in this work will be made available through the BALSA database (`https://balsa.wustl.edu/`) upon manuscript acceptance. Amongst other information, the dataset will include interactive visualizations of the send-receive asymmetry cortical projections shown in Fig 3 and tables detailing the send-receive asymmetry obtained for all cortical regions. We will also provide a MATLAB demonstration script that uses this data to systematically reproduce our key findings.

Functions to compute navigation efficiency, diffusion efficiency and search information are available as part of the Brain Connectivity Toolbox (`https://sites.google.com/site/bctnet/`). Further analyses and computations were performed using MRtrix3 (`www.mrtrix.org/`), SPM12 (`https://www.fil.ion.ucl.ac.uk/spm/software/spm12/`) or custom MATLAB code that will be made available upon acceptance of this manuscript, as per described in the *Materials and Methods*.


[1] O. Sporns, G. Tononi, and R. Kötter, "The human connectome: A structural description of the human brain," *PLoS Comput Biol*, vol. 1, p. e42, Sep 2005.

[2] P. Hagmann, L. Cammoun, X. Gigandet, R. Meuli, C. J. Honey, V. J. Wedeen, and O. Sporns, "Mapping the structural core of human cerebral cortex," *PLoS Biol*, vol. 6, p. e159, Jul 2008.

[3] C. J. Honey, O. Sporns, L. Cammoun, X. Gigandet, J. P. Thiran, R. Meuli, and P. Hagmann, "Predicting human resting-state functional connectivity from structural connectivity," *Proc Natl Acad Sci U S A*, vol. 106, pp. 2035–40, Feb 2009.

[4] R. F. Betzel, L. Byrge, Y. He, J. Goñi, X.-N. Zuo, and O. Sporns, "Changes in structural and functional connectivity among resting-state networks across the human lifespan," *Neuroimage*, vol. 102 Pt 2, pp. 345–57, Nov 2014.

[5] B. Mišić, R. F. Betzel, M. A. de Reus, M. P. van den Heuvel, M. G. Berman, A. R. McIntosh, and O. Sporns, "Network-level structure-function relationships in human neocortex," *Cereb Cortex*, vol. 26, pp. 3285–96, Jul 2016.

[6] E. Amico and J. Goñi, "Mapping hybrid functional-structural connectivity traits in the human connectome," *Netw Neurosci*, vol. 2, no. 3, pp. 306–322, 2018.

[7] S. B. Laughlin and T. J. Sejnowski, "Communication in neuronal networks," *Science*, vol. 301, pp. 1870–4, Sep 2003.

[8] J. Goñi, M. P. van den Heuvel, A. Avena-Koenigsberger, N. Velez de Mendizabal, R. F. Betzel, A. Griffa, P. Hagmann, B. Corominas-Murtra, J.-P. Thiran, and O. Sporns, "Resting-brain functional connectivity predicted by analytic measures of network communication," *Proc Natl Acad Sci U S A*, vol. 111, pp. 833–8, Jan 2014.

[9] A. Avena-Koenigsberger, B. Misic, and O. Sporns, "Communication dynamics in complex brain networks," *Nat Rev Neurosci*, vol. 19, pp. 17–33, Dec 2017.

[10] G. Hahn, A. Ponce-Alvarez, G. Deco, A. Aertsen, and A. Kumar, "Portraits of communication in neuronal networks," *Nat Rev Neurosci*, Dec 2018.

[11] M. Rubinov and O. Sporns, "Complex network measures of brain connectivity: uses and interpretations," *Neuroimage*, vol. 52, pp. 1059–69, Sep 2010.

[12] E. Bullmore and O. Sporns, "Complex brain networks: graph theoretical analysis of structural and functional systems," *Nature Reviews Neuroscience*, vol. 10, no. 3, pp. 186–198

[13] E. Bullmore and O. Sporns, "The economy of brain network organization," *Nat Rev Neurosci*, vol. 13, pp. 336–49, Apr 2012.

[14] B. Misic, R. F. Betzel, A. Griffa, M. A. de Reus, Y. He, X.-N. Zuo, M. P. van den Heuvel, P. Hagmann, O. Sporns, and R. J. Zatorre, "Network-based asymmetry of the human auditory system," *bioRxiv*, p. 251827, 2018.

[15] C. Seguin, M. P. van den Heuvel, and A. Zalesky, "Navigation of brain networks," *Proc Natl Acad Sci U S A*, vol. 115, pp. 6297–6302, 06 2018.

[16] M. Boguna, D. Krioukov, and K. C. Claffy, "Navigability of complex networks," *Nature Physics*, vol. 5, no. 1, pp. 74–80

[17] A. Allard and M. Serrano, "Navigable maps of structural brain networks across species," *arXiv preprint arXiv:1801.06079*, 2018.

[18] B. Mišić, R. F. Betzel, A. Nematzadeh, J. Goñi, A. Griffa, P. Hagmann, A. Flammini, Y.-Y. Ahn, and O. Sporns, "Cooperative and competitive spreading dynamics on the human connectome," *Neuron*, vol. 86, pp. 1518–29, Jun 2015.

[19] J. C. Worrell, J. Rumschlag, R. F. Betzel, O. Sporns, and B. Mišić, "Optimized connectome architecture for sensory-motor integration," *Netw Neurosci*, vol. 1, no. 4, pp. 415–430, 2018.

[20] E. Estrada and N. Hatano, "Communicability in complex networks," *Phys Rev E Stat Nonlin Soft Matter Phys*, vol. 77, p. 036111, Mar 2008.

[21] J. J. Crofts and D. J. Higham, "A weighted communicability measure applied to complex brain networks," *J R Soc Interface*, vol. 6, pp. 411–4, Apr 2009.

[22] J. Andreotti, K. Jann, L. Melie-Garcia, S. Giezendanner, E. Abela, R. Wiest, T. Dierks, and A. Federspiel, "Validation of network communicability metrics for the analysis of brain structural networks," *PLoS One*, vol. 9, no. 12, p. e115503, 2014.

[23] N. Masuda, M. A. Porter, and R. Lambiotte, "Random walks and diffusion on networks," *Physics reports*, vol. 716, pp. 1–58, 2017.

[24] J. Goñi, A. Avena-Koenigsberger, N. Velez de Mendizabal, M. P. van den Heuvel, R. F. Betzel, and O. Sporns, "Exploring the morphospace of communication efficiency in complex networks," *PLoS One*, vol. 8, no. 3, p. e58070, 2013.

[25] F. Abdelnour, H. U. Voss, and A. Raj, "Network diffusion accurately models the relationship between structural and functional brain connectivity networks," *Neuroimage*, vol. 90, pp. 335–47, Apr 2014.

[26] A. Avena-Koenigsberger, X. Yan, A. Kolchinsky, M. van den Heuvel, P. Hagmann, and O. Sporns, "A spectrum of routing strategies for brain networks," *PLoS Comput Biol*, vol. 15, p. e1006833, Mar 2019.

[27] K. J. Friston, "Functional and effective connectivity: a review," *Brain Connect*, vol. 1, no. 1, pp. 13–36, 2011.

[28] M. Gilson, R. Moreno-Bote, A. Ponce-Alvarez, P. Ritter, and G. Deco, "Estimation of directed effective connectivity from fmri functional connectivity hints at asymmetries of cortical connectome," *PLoS Comput Biol*, vol. 12, p. e1004762, Mar 2016.

[29] L. L. Gollo, J. A. Roberts, and L. Cocchi, "Mapping how local perturbations influence systems-level brain dynamics," *Neuroimage*, Jan 2017.

[30] A. Fornito, A. Zalesky, and E. T. Bullmore, *Fundamentals of brain network analysis*. 2016.

[31] Kleinberg, "Navigation in a small world," *Nature*, vol. 406, p. 845, Aug 2000.

[32] M. Rosvall, A. Grönlund, P. Minnhagen, and K. Sneppen, "Searchability of networks," *Phys Rev E Stat Nonlin Soft Matter Phys*, vol. 72, p. 046117, Oct 2005.

[33] D. C. Van Essen, S. M. Smith, D. M. Barch, T. E. J. Behrens, E. Yacoub, K. Ugurbil, and WU-Minn HCP Consortium, "The wu-minn human connectome project: an overview," *Neuroimage*, vol. 80, pp. 62–79, Oct 2013.

[34] A. Zalesky, A. Fornito, L. Cocchi, L. L. Gollo, M. P. van den Heuvel, and M. Breakspear, "Connectome sensitivity or specificity: which is more important?," *Neuroimage*, Jun 2016.

[35] J. Sepulcre, M. R. Sabuncu, T. B. Yeo, H. Liu, and K. A. Johnson, "Stepwise connectivity of the modal cortex reveals the multimodal organization of the human brain," *J Neurosci*, vol. 32, pp. 10649–61, Aug 2012.

[36] M. F. Glasser, T. S. Coalson, E. C. Robinson, C. D. Hacker, J. Harwell, E. Yacoub, K. Ugurbil, J. Andersson, C. F. Beckmann, M. Jenkinson, S. M. Smith, and D. C. Van Essen, "A multi-modal parcellation of human cerebral cortex," *Nature*, vol. 536, pp. 171–178, 08 2016.

[37] G. Zamora-López, C. Zhou, and J. Kurths, "Cortical hubs form a module for multisensory integration on top of the hierarchy of cortical networks," *Front Neuroinform*, vol. 4, p. 1, 2010.

[38] D. S. Margulies, S. S. Ghosh, A. Goulas, M. Falkiewicz, J. M. Huntenburg, G. Langs, G. Bezgin, S. B. Eickhoff, F. X. Castellanos, M. Petrides, E. Jefferies, and J. Smallwood, "Situating the default-mode network along a principal gradient of macroscale cortical organization," *Proc Natl Acad Sci U S A*, vol. 113, pp. 12574–12579, 11 2016.

[39] E. M. Gordon, C. J. Lynch, C. Gratton, T. O. Laumann, A. W. Gilmore, D. J. Greene, M. Ortega, A. L. Nguyen, B. L. Schlaggar, S. E. Petersen, N. U. F. Dosenbach, and S. M. Nelson, "Three distinct sets of connector hubs integrate human brain function," *Cell Rep*, vol. 24, pp. 1687–1695.e4, Aug 2018.

[40] J. M. Huntenburg, P.-L. Bazin, and D. S. Margulies, "Large-scale gradients in human cortical organization," *Trends Cogn Sci*, vol. 22, pp. 21–31, Jan 2018.

[41] B. T. T. Yeo, F. M. Krienen, J. Sepulcre, M. R. Sabuncu, D. Lashkari, M. Hollinshead, J. L. Roffman, J. W. Smoller, L. Zöllei, J. R. Polimeni, B. Fischl, H. Liu, and R. L. Buckner, "The organization of the human cerebral cortex estimated by intrinsic functional connectivity," *J Neurophysiol*, vol. 106, pp. 1125–65, Sep 2011.

[42] K. J. Friston, J. Kahan, B. Biswal, and A. Razi, "A dcm for resting state fmri," *Neuroimage*, vol. 94, pp. 396–407, Jul 2014.

[43] A. Razi, J. Kahan, G. Rees, and K. J. Friston, "Construct validation of a dcm for resting state fmri," *Neuroimage*, vol. 106, pp. 1–14, Feb 2015.

[44] M. P. van den Heuvel, E. T. Bullmore, and O. Sporns, "Comparative connectomics," *Trends Cogn Sci*, vol. 20, pp. 345–61, May 2016.

[45] A.-S. Chiang, C.-Y. Lin, C.-C. Chuang, H.-M. Chang, C.-H. Hsieh, C.-W. Yeh, C.-T. Shih, J.-J. Wu, G.-T. Wang, Y.-C. Chen, C.-C. Wu, G.-Y. Chen, Y.-T. Ching, P.-C. Lee, C.-Y. Lin, H.-H. Lin, C.-C. Wu, H.-W. Hsu, Y.-A. Huang, J.-Y. Chen, H.-J. Chiang, C.-F. Lu, R.-F. Ni, C.-Y. Yeh, and J.-K. Hwang, "Three-dimensional reconstruction of brain-wide wiring networks in drosophila at single-cell resolution," *Curr Biol*, vol. 21, pp. 1–11, Jan 2011.

[46] C.-T. Shih, O. Sporns, S.-L. Yuan, T.-S. Su, Y.-J. Lin, C.-C. Chuang, T.-Y. Wang, C.-C. Lo, R. J. Greenspan, and A.-S. Chiang, "Connectomics-based analysis of information flow in the drosophila brain," *Curr Biol*, vol. 25, pp. 1249–58, May 2015.

[47] S. W. Oh, J. A. Harris, L. Ng, B. Winslow, N. Cain, S. Mihalas, Q. Wang, C. Lau, L. Kuan, A. M. Henry, M. T. Mortrud, B. Ouellette, T. N. Nguyen, S. A. Sorensen, C. R. Slaughterbeck, W. Wakeman, Y. Li, D. Feng, A. Ho, E. Nicholas, K. E. Hirokawa, P. Bohn, K. M. Joines, H. Peng, M. J. Hawrylycz, J. W. Phillips, J. G. Hohmann, P. Wohnoutka, C. R. Gerfen, C. Koch, A. Bernard, C. Dang, A. R. Jones, and H. Zeng, "A mesoscale connectome of the mouse brain," *Nature*, vol. 508, pp. 207–14, Apr 2014.

[48] M. Rubinov, R. J. F. Ypma, C. Watson, and E. T. Bullmore, "Wiring cost and topological participation of the mouse brain connectome," *Proc Natl Acad Sci U S A*, vol. 112, pp. 10032–7, Aug 2015.

[49] N. T. Markov, M. M. Ercsey-Ravasz, A. R. Ribeiro Gomes, C. Lamy, L. Magrou, J. Vezoli, P. Misery, A. Falchier, R. Quilodran, M. A. Gariel, J. Sallet, R. Gamanut, C. Huissoud, S. Clavagnier, P. Giroud, D. Sappey-Marinier, P. Barone, C. Dehay, Z. Toroczkai, K. Knoblauch, D. C. Van Essen, and H. Kennedy, "A weighted and directed interareal connectivity matrix for macaque cerebral cortex," *Cereb Cortex*, vol. 24, pp. 17–36, Jan 2014.

[50] D. J. Felleman and D. C. Van Essen, "Distributed hierarchical processing in the primate cerebral cortex," *Cereb Cortex*, vol. 1, no. 1, pp. 1–47, 1991.

[51] P. Kale, A. Zalesky, and L. L. Gollo, "Estimating the impact of structural directionality: How reliable are undirected connectomes?," *Netw Neurosci*, vol. 2, no. 2, pp. 259–284, 2018.

[52] N. T. Markov, M. Ercsey-Ravasz, D. C. Van Essen, K. Knoblauch, Z. Toroczkai, and H. Kennedy, "Cortical high-density counterstream architectures," *Science*,

vol. 342, p. 1238406, Nov 2013.

[53] J. B. Burt, M. Demirtaş, W. J. Eckner, N. M. Navejar, J. L. Ji, W. J. Martin, A. Bernacchia, A. Anticevic, and J. D. Murray, "Hierarchy of transcriptomic specialization across human cortex captured by structural neuroimaging topography," *Nat Neurosci*, vol. 21, pp. 1251–1259, Sep 2018.

[54] R. Chaudhuri, K. Knoblauch, M.-A. Gariel, H. Kennedy, and X.-J. Wang, "A large-scale circuit mechanism for hierarchical dynamical processing in the primate cortex," *Neuron*, vol. 88, pp. 419–31, Oct 2015.

[55] L. Cocchi, M. V. Sale, L. L Gollo, P. T. Bell, V. T. Nguyen, A. Zalesky, M. Breakspear, and J. B. Mattingley, "A hierarchy of timescales explains distinct effects of local inhibition of primary visual cortex and frontal eye fields," *Elife*, vol. 5, Sep 2016.

[56] G. Deco and M. L. Kringelbach, "Hierarchy of information processing in the brain: A novel 'intrinsic ignition' framework," *Neuron*, vol. 94, pp. 961–968, Jun 2017.

[57] M. Demirtaş, J. B. Burt, M. Helmer, J. L. Ji, B. D. Adkinson, M. F. Glasser, D. C. Van Essen, S. N. Sotiropoulos, A. Anticevic, and J. D. Murray, "Hierarchical heterogeneity across human cortex shapes large-scale neural dynamics," *Neuron*, Feb 2019.

[58] H. Almgren, F. Van de Steen, S. Kühn, A. Razi, K. Friston, and D. Marinazzo, "Variability and reliability of effective connectivity within the core default mode network: A multi-site longitudinal spectral dcm study," *Neuroimage*, vol. 183, pp. 757–768, Dec 2018.

[59] D. Bernal-Casas, H. J. Lee, A. J. Weitz, and J. H. Lee, "Studying brain circuit function with dynamic causal modeling for optogenetic fmri," *Neuron*, vol. 93, pp. 522–532.e5, Feb 2017.

[60] M. W. Cole, D. S. Bassett, J. D. Power, T. S. Braver, and S. E. Petersen, "Intrinsic and task-evoked network architectures of the human brain," *Neuron*, vol. 83, pp. 238–51, Jul 2014.

[61] T. Ito, K. R. Kulkarni, D. H. Schultz, R. D. Mill, R. H. Chen, L. I. Solomyak, and M. W. Cole, "Cognitive task information is transferred between brain regions via resting-state network topology," *Nat Commun*, vol. 8, p. 1027, 10 2017.

[62] A. Razi, M. L. Seghier, Y. Zhou, P. McColgan, P. Zeidman, H.-J. Park, O. Sporns, G. Rees, and K. J. Friston, "Large-scale dcms for resting-state fmri," *Netw Neurosci*, vol. 1, no. 3, pp. 222–241, 2017.

[63] A. A. Sokolov, P. Zeidman, M. Erb, P. Ryvlin, M. A. Pavlova, and K. J. Friston, "Linking structural and effective brain connectivity: structurally informed parametric empirical bayes (si-peb)," *Brain Struct Funct*, Oct 2018.

[64] B. Mišić, O. Sporns, and A. R. McIntosh, "Communication efficiency and congestion of signal traffic in large-scale brain networks," *PLoS Comput Biol*, vol. 10, p. e1003427, Jan 2014.

[65] U. Tipnis, E. Amico, M. Ventresca, and J. Goñi, "Modeling communication processes in the human connectome through cooperative learning," *IEEE Transactions on Network Science and Engineering*, 02 2018.

[66] A. K. Seth, A. B. Barrett, and L. Barnett, "Granger causality analysis in neuroscience and neuroimaging," *J Neurosci*, vol. 35, pp. 3293–7, Feb 2015.

[67] J. Kim, W. Zhu, L. Chang, P. M. Bentler, and T. Ernst, "Unified structural equation modeling approach for the analysis of multisubject, multivariate functional mri data," *Hum Brain Mapp*, vol. 28, pp. 85–93, Feb 2007.

[68] K. H. Maier-Hein, P. F. Neher, J.-C. Houde, M.-A. Côté, E. Garyfallidis, J. Zhong, M. Chamberland, F.-C. Yeh, Y.-C. Lin, Q. Ji, W. E. Reddick, J. O. Glass, D. Q. Chen, Y. Feng, C. Gao, Y. Wu, J. Ma, H. Renjie, Q. Li, C.-F. Westin, S. Deslauriers-Gauthier, J. O. O. González, M. Paquette, S. St-Jean, G. Girard, F. Rheault, J. Sidhu, C. M. W. Tax, F. Guo, H. Y. Mesri, S. Dávid, M. Froeling, A. M. Heemskerk, A. Leemans, A. Boré, B. Pinsard, C. Bedetti, M. Desrosiers, S. Brambati, J. Doyon, A. Sarica, R. Vasta, A. Cerasa, A. Quattrone, J. Yeatman, A. R. Khan, W. Hodges, S. Alexander, D. Romascano, M. Barakovic, A. Auría, O. Esteban, A. Lemkaddem, J.-P. Thiran, H. E. Cetingul, B. L. Odry, B. Mailhe, M. S. Nadar, F. Pizzagalli, G. Prasad, J. E. Villalon-Reina, J. Galvis, P. M. Thompson, F. D. S. Requejo, P. L. Laguna, L. M. Lacerda, R. Barrett, F. Dell'Acqua, M. Catani, L. Petit, E. Caruyer, A. Daducci, T. B. Dyrby, T. Holland-Letz, C. C. Hilgetag, B. Stieltjes, and M. Descoteaux, "The challenge of mapping the human connectome based on diffusion tractography," *Nat Commun*, vol. 8, p. 1349, Nov 2017.

[69] T. Sarwar, K. Ramamohanarao, and A. Zalesky, "Mapping connectomes with diffusion mri: deterministic or probabilistic tractography?," *Magn Reson Med*, vol. 81, pp. 1368–1384, Feb 2019.

[70] M. F. Glasser, S. N. Sotiropoulos, J. A. Wilson, T. S. Coalson, B. Fischl, J. L. Andersson, J. Xu, S. Jbabdi, M. Webster, J. R. Polimeni, D. C. Van Essen, M. Jenkinson, and WU-Minn HCP Consortium, "The minimal preprocessing pipelines for the human connectome project," *Neuroimage*, vol. 80, pp. 105–24, Oct 2013.

[71] S. N. Sotiropoulos, S. Jbabdi, J. Xu, J. L. Andersson, S. Moeller, E. J. Auerbach, M. F. Glasser, M. Hernandez, G. Sapiro, M. Jenkinson, D. A. Feinberg, E. Yacoub, C. Lenglet, D. C. Van Essen, K. Ugurbil, T. E. J. Behrens, and WU-Minn HCP Consortium, "Advances in diffusion mri acquisition and processing in the human connectome project," *Neuroimage*, vol. 80, pp. 125–43, Oct 2013.

[72] A. Zalesky, A. Fornito, I. H. Harding, L. Cocchi, M. Yücel, C. Pantelis, and E. T. Bullmore, "Whole-brain anatomical networks: does the choice of nodes matter?," *Neuroimage*, vol. 50, pp. 970–83, Apr 2010.

[73] J.-D. Tournier, F. Calamante, and A. Connelly, "Mrtrix: Diffusion tractography in crossing fiber regions," *International Journal of Imaging Systems and Technology*, vol. 22, 03 2012.

[74] N. T. Markov, M. Ercsey-Ravasz, C. Lamy, A. R. Ribeiro Gomes, L. Magrou, P. Misery, P. Giroud, P. Barone, C. Dehay, Z. Toroczkai, K. Knoblauch, D. C. Van Essen, and H. Kennedy, "The role of long-range connections on the specificity of the macaque interareal cortical network," *Proc Natl Acad Sci U S A*, vol. 110, pp. 5187–92, Mar 2013.

[75] A. Avena-Koenigsberger, B. Mišić, R. X. Hawkins, A. Griffa, P. Hagmann, J. Goñi, and O. Sporns, "Path ensembles and a tradeoff between communication efficiency and resilience in the human connectome," *Brain Structure and Function*, pp. 1–16, 2016.

[76] H. Zhou, "Network landscape from a brownian particle's perspective," *Phys Rev E Stat Nonlin Soft Matter Phys*, vol. 67, p. 041908, Apr 2003.

[77] S. Maslov and K. Sneppen, "Specificity and stability in

topology of protein networks," *Science*, vol. 296, pp. 910–3, May 2002.

[78] R. F. Betzel, A. Avena-Koenigsberger, J. Goñi, Y. He, M. A. de Reus, A. Griffa, P. E. Vértes, B. Mišic, J.-P. Thiran, P. Hagmann, M. van den Heuvel, X.-N. Zuo, E. T. Bullmore, and O. Sporns, "Generative models of the human connectome," *Neuroimage*, vol. 124, pp. 1054–64, Jan 2016.

## SUPPLEMENTARY INFORMATION

### Note 1: Consistency of sender-neutral-receiver classification of cortical regions across communication measures

Extending our analyses of correlations between send-receive asymmetries across communication measures, we compared the sender-neutral-receiver classifications of cortical regions obtained from navigation efficiency, diffusion efficiency and search information (Table S1). As expected by their mutual dependency on random walk processes, classifications for send-receive asymmetries under diffusion efficiency and search information were tightly related (76% accuracy, Table S1c). While classification under navigation showed less agreement with the other measures (46% and 44% accuracy for diffusion and search information, respectively; Table S1a,b), the obtained three-way classification accuracy remained larger than the 33% baseline expected by chance.

We further explored this relationship by considering two-way classifications of regions into sender or not sender, and receiver or not receiver. This allowed us to assess the statistical significance of the association between the classifications from two communication measures by using Fisher's exact test. The significance of the obtained P-values further supports the classification consistency across communication measures (Table S1d-i).

### Note 2: Randomized connectomes

We used three families of randomized connectomes: i) topologically randomized (rewired) networks, ii) topologically randomized cost-preserving networks and iii) spatially randomized (repositioned) networks. For $K$ subjects, each individual connectome was used to generate ensembles of 1,000 surrogate networks for each family. Computing communication measures for these networks resulted in 1,000 sets of $C_{N\times N\times K}$ null communication efficiency matrices, per family, per communication measure. These sets were downsampled to subsystem resolution and used to compute the correlation between effective connectivity and null network send-receive communication asymmetries. Non-parametric P-values testing the hypothesis of a lack of difference between empirical and null correlations were computed as the proportion of times the communication asymmetry of null networks yielded stronger correlations than the one obtained for the empirical connectome.

Topologically randomized networks were computed using the Maslov-Sneppen rewiring routine [77] implemented in the Brain Connectivity Toolbox [11]. In this procedure, each connection was swapped between nodes once (on average), while maintaining the network's original degree distribution and ensuring it remained connected.

One disadvantage of topologically randomized net-

works is the introduction of a disproportionate number of long-range connections, resulting in null networks with markedly increased wiring cost compared to the empirical network. To address this issue, we first computed the empirical wiring cost of a network as the sum of Euclidean distances between its connected nodes [78]. We then generated cost-preserving topologically randomized networks by adding a constraint to the Maslov-Sneppen routine, namely that connection swaps must not alter the original network's cost by more than 1mm. Previous studies report that this leads to surrogate networks that match empirical wiring cost within a 0.1% error margin [15].

Spatially randomized networks are relevant for navigation, which routes information based on local knowledge of network geometry. They are constructed by randomly swapping the spatial positioning of nodes, while maintaining network topology unaltered.

| | S | N | R |
|---|---|---|---|
| S | 86 | 15 | 24 |
| N | 35 | 20 | 36 |
| R | 61 | 22 | 61 |

**(a)** Navigation (rows) and diffusion (columns): $Acc = 0.46$.

| | S | N | R |
|---|---|---|---|
| S | 70 | 15 | 40 |
| N | 27 | 13 | 51 |
| R | 43 | 22 | 79 |

**(b)** Navigation and SI: $Acc = 0.44$.

| | S | N | R |
|---|---|---|---|
| S | 140 | 37 | 5 |
| N | 0 | 13 | 44 |
| R | 0 | 0 | 121 |

**(c)** Diffusion and SI: $Acc = 0.76$.

| | S | $\neg S$ |
|---|---|---|
| S | 129 | 101 |
| $\neg S$ | 49 | 81 |

**(d)** Nav & diff: $Acc = 0.58$, $P = 0.001$.

| | R | $\neg R$ |
|---|---|---|
| R | 157 | 56 |
| $\neg R$ | 82 | 65 |

**(e)** Nav & diff: $Acc = 0.67$, $P = 6 \times 10^{-4}$.

| | S | $\neg S$ |
|---|---|---|
| S | 155 | 75 |
| $\neg S$ | 65 | 65 |

**(f)** Nav & SI: $Acc = 0.61$, $P = 0.002$.

| | R | $\neg R$ |
|---|---|---|
| R | 124 | 89 |
| $\neg R$ | 66 | 81 |

**(g)** Nav & SI: $Acc = 0.57$, $P = 0.014$.

| | S | $\neg S$ |
|---|---|---|
| S | 178 | 0 |
| $\neg S$ | 42 | 140 |

**(h)** Diff & SI: $Acc = 0.88$, $P = 3 \times 10^{-62}$.

| | R | $\neg R$ |
|---|---|---|
| R | 190 | 49 |
| $\neg R$ | 0 | 121 |

**(i)** Diff & SI: $Acc = 0.86$, $P = 5 \times 10^{-56}$.

**TABLE S1.** Comparison of the classification of cortical regions as senders (S), neutral (N) and receivers (R) across network communication measures. The classification accuracy ($Acc$) is computed as the sum of values in the main diagonal (number of consistently classified regions) divided by the sum of values in the table (total number of regions). **(a-c)** Three-way contingency tables of the classification obtained from the send-receive asymmetries of two communication measures. Measures listed first and second in the captions have their classes displayed in the rows and columns of the tables, respectively. **(d-i)** Two-way contingency tables of the classification obtained from the send-receive asymmetries of two communication measures. In this case, for each pair of measures, regions are classified as sender (S) or not sender ($\neg S$), and receiver (R) or not receiver ($\neg R$). P-values obtained from Fisher's exact test were used to examine the significance of the association between the classifications of two measures.

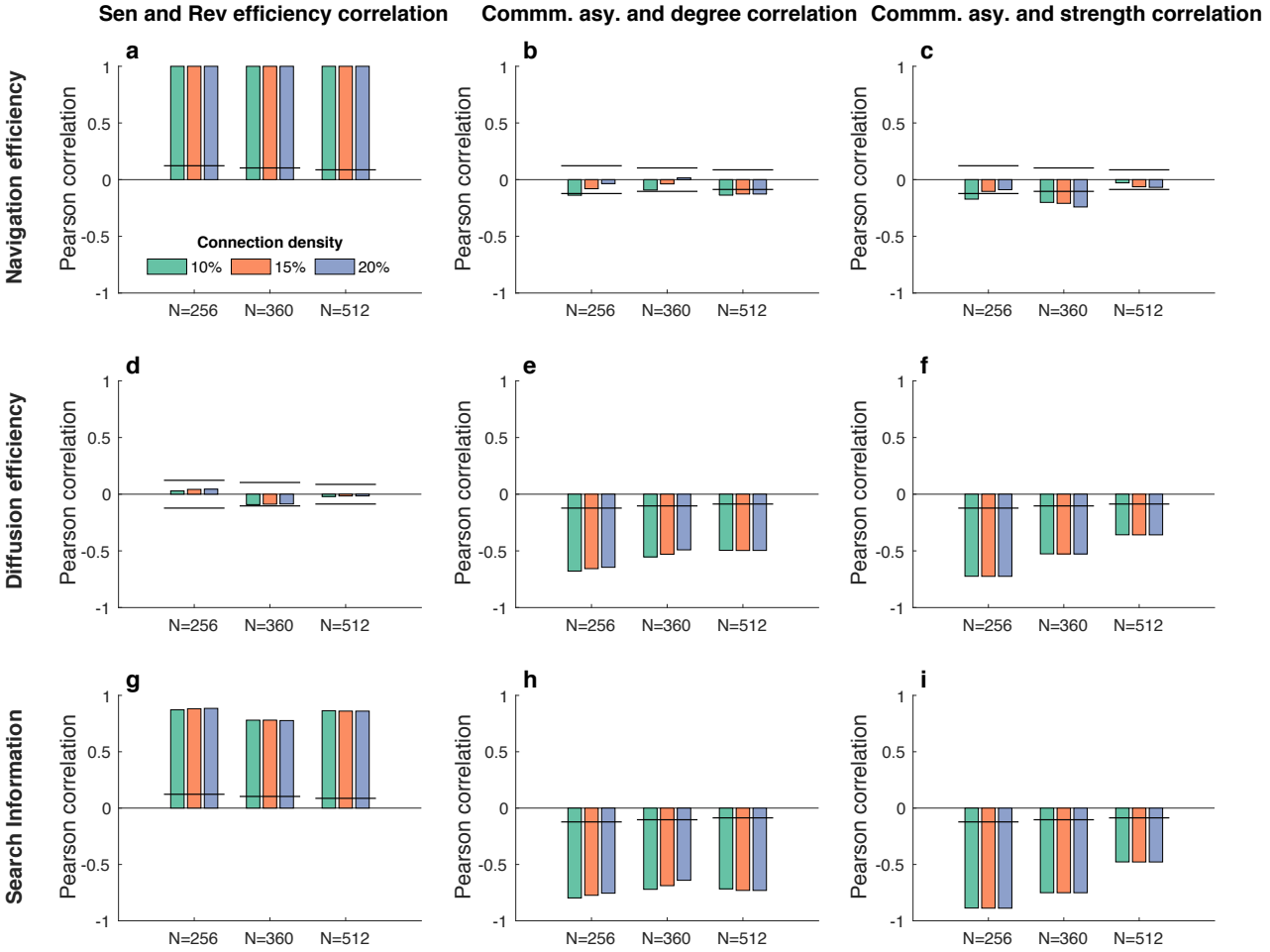


**FIG. S1.** Replication analyses regarding sending efficiency, receiving efficiency and send-receive communication asymmetry for $N = 256, 360, 512$ parcellation resolutions and 10%, 15% and 20% connection density thresholds. Vertical axes indicate the Pearson correlation's $r$, while black horizontal lines mark the effect size correspondent to a correlation with $P = 0.05$ for each $N$. **(a)** Correlation between sending and receiving navigation efficiencies. **(b)** Correlation between regional navigation asymmetry and node degree (averaged across the connectomes of all participants). **(c)** Same as b, but for node strength. **(d-f)** Same as a-c, but for diffusion efficiency. **(g-i)** Same as a-c, but for search information.

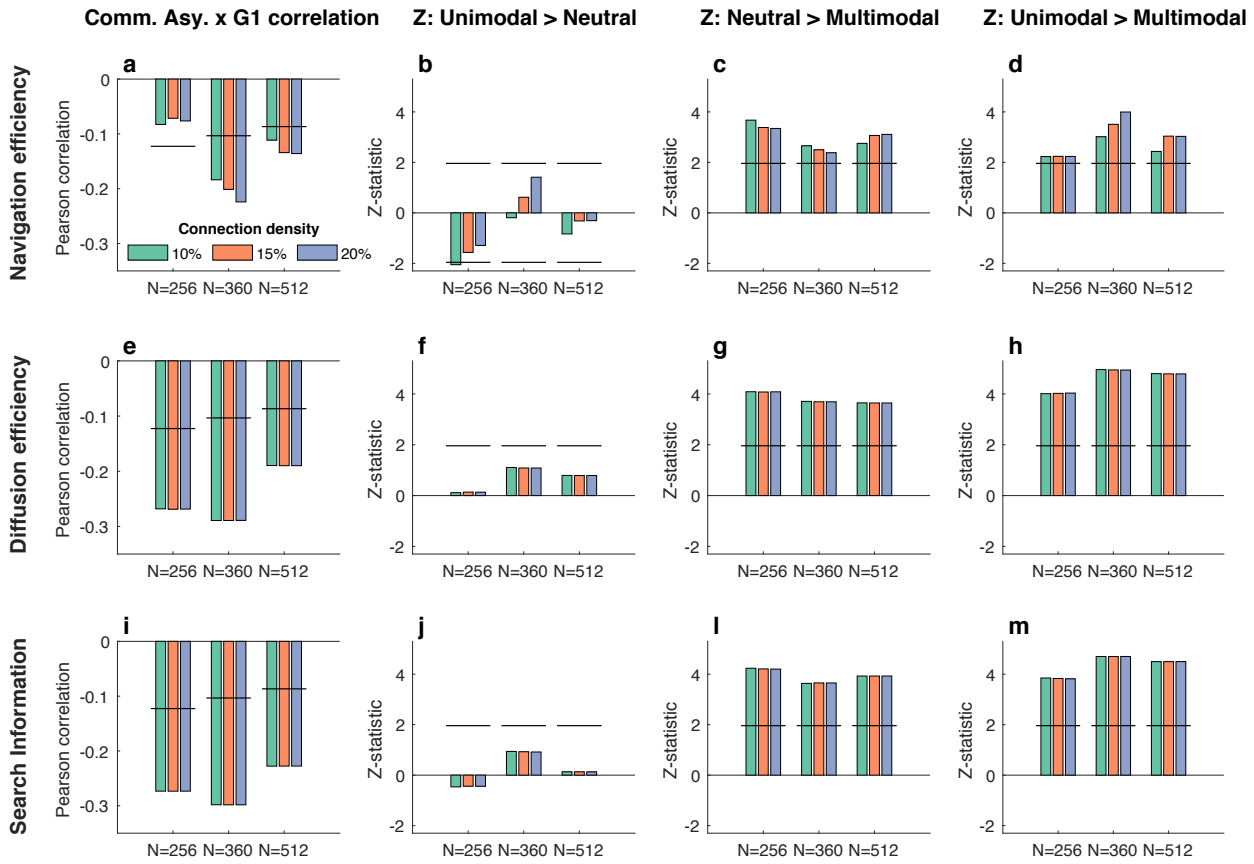


**FIG. S2.** Replication analyses regarding the relationship between communication asymmetry and functional heterogeneity for $N = 256, 360, 512$ parcellation resolutions and 10%, 15% and 20% connection density thresholds. The obtained results are consistent across parcellations and connection densities, with the exception of the lack of correlation between send-receive asymmetry and the gradient of functional heterogeneity for $N = 256$. **(a)** Pearson correlation between regional navigation asymmetry and functional heterogeneity. Black horizontal lines mark the effect size correspondent to a correlation with $P = 0.05$ for each $N$. **(b)** Z-statistic from a two-sided Wilcoxon test evaluating the hypothesis that the median navigation asymmetry of unimodal regions is larger than that of neutral regions. Black horizontal lines mark the value of a Z-statistic correspondent to $P = 0.05$. **(c)** Same as b, but for neutral and multimodal regions. **(d)** Same as b, but for unimodal and multimodal regions. **(e-h)** Same as a-d, but for diffusion efficiency. **(i-m)** Same as a-d, but for search information.

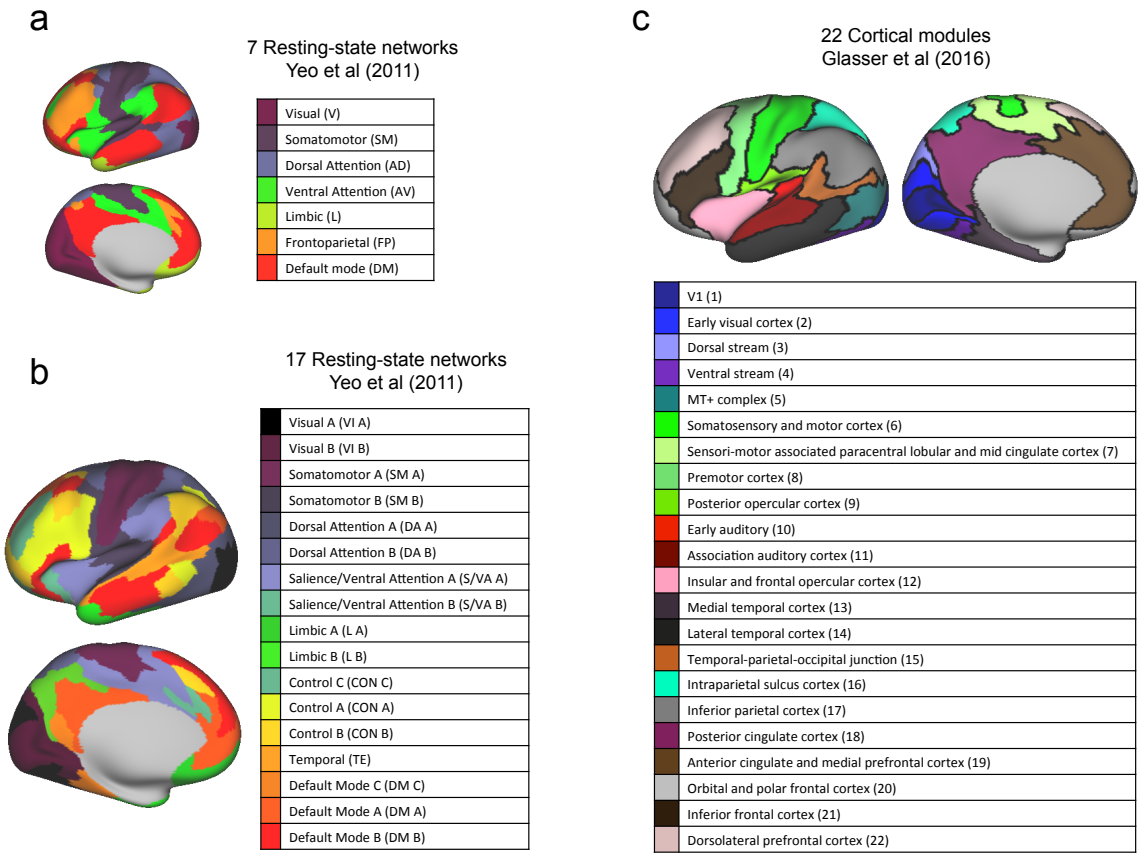


**FIG. S3.** Definition of the $M = 7, 17, 22$ cortical subsystems utilized in sections *Send-receive communication asymmetries of cortical subsystems Send-receive communication asymmetry and effective connectivity.*

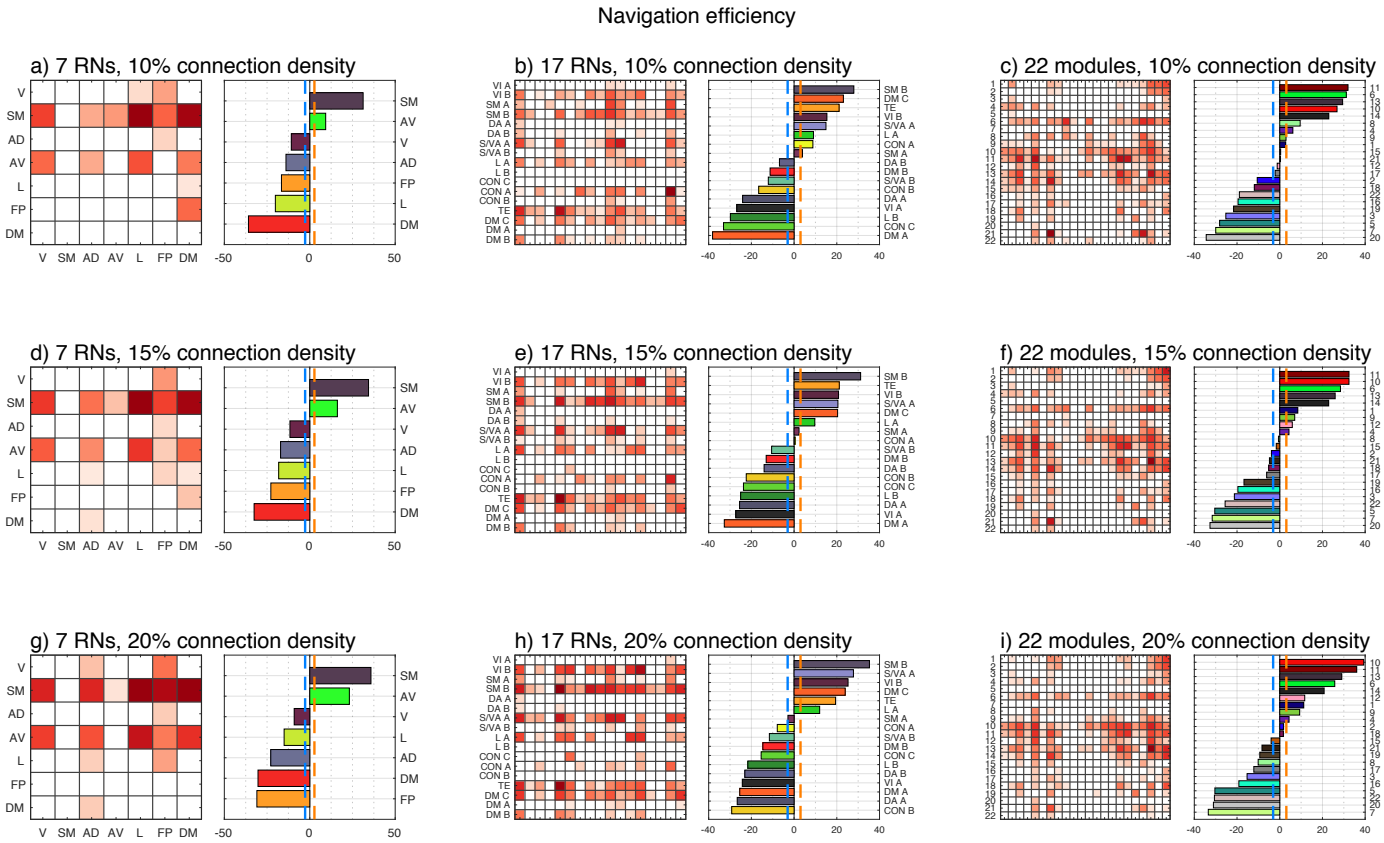


**FIG. S4.** Send-receive navigation asymmetry of cortical subsystems for $M = 7, 17, 22$ and 10%, 15% and 20% connection density thresholds. Send-receive asymmetry matrices were thresholded to display only statistically significant values, while accounting for multiple comparisons. For ease of visualization and without loss of information (since $A(i,j) = -A(j,i)$), negative values were omitted. Thus, $A(i,j) > 0$ denotes that communication takes place more efficiently from $i$ to $j$ than from $j$ to $i$.

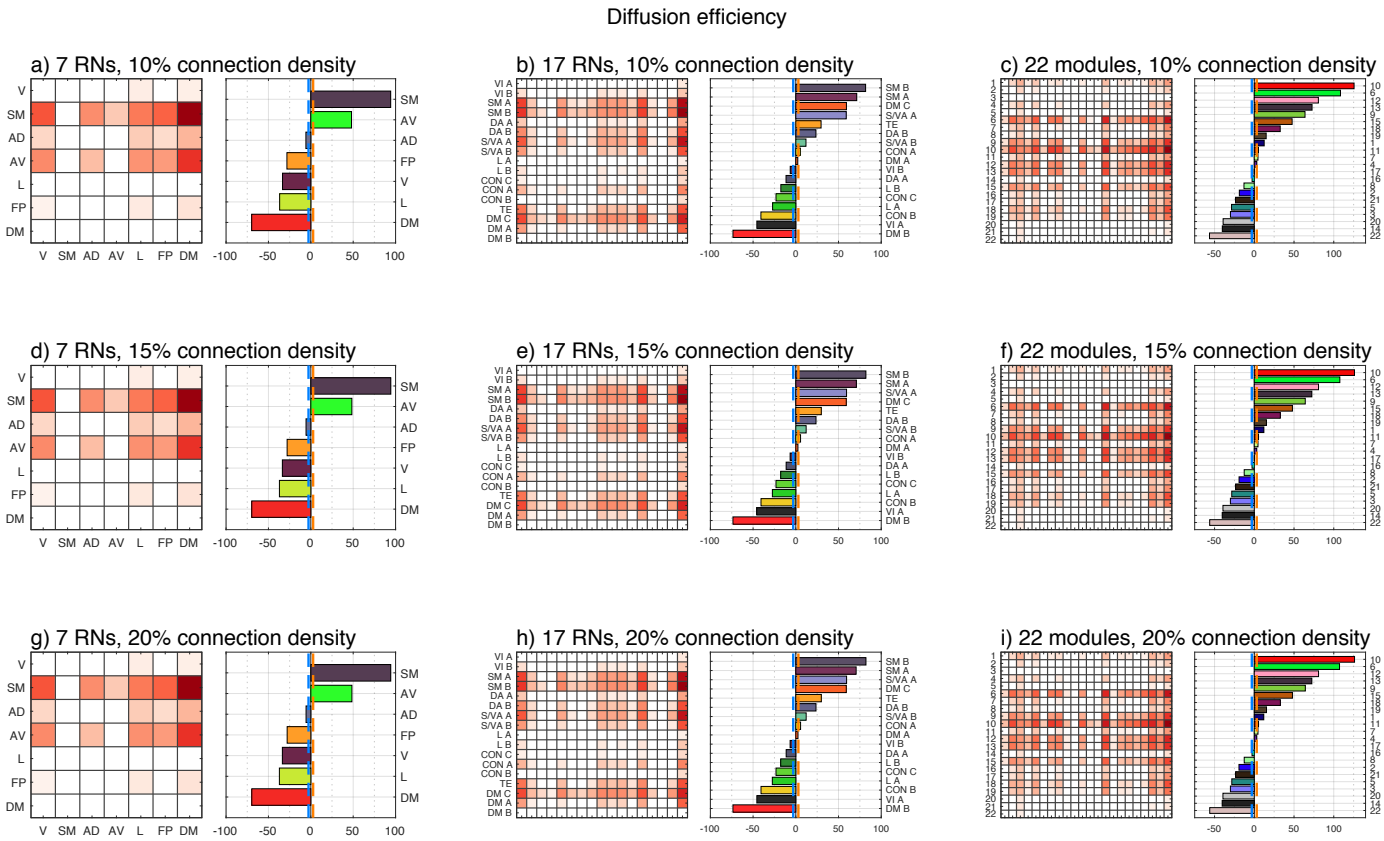


**FIG. S5.** Send-receive diffusion asymmetry of cortical subsystems for $M = 7, 17, 22$ and 10%, 15% and 20% connection density thresholds. Send-receive asymmetry matrices were thresholded to display only statistically significant values, while accounting for multiple comparisons. For ease of visualization and without loss of information (since $A(i, j) = -A(j, i)$), negative values were omitted. Thus, $A(i, j) > 0$ denotes that communication takes place more efficiently from $i$ to $j$ than from $j$ to $i$.

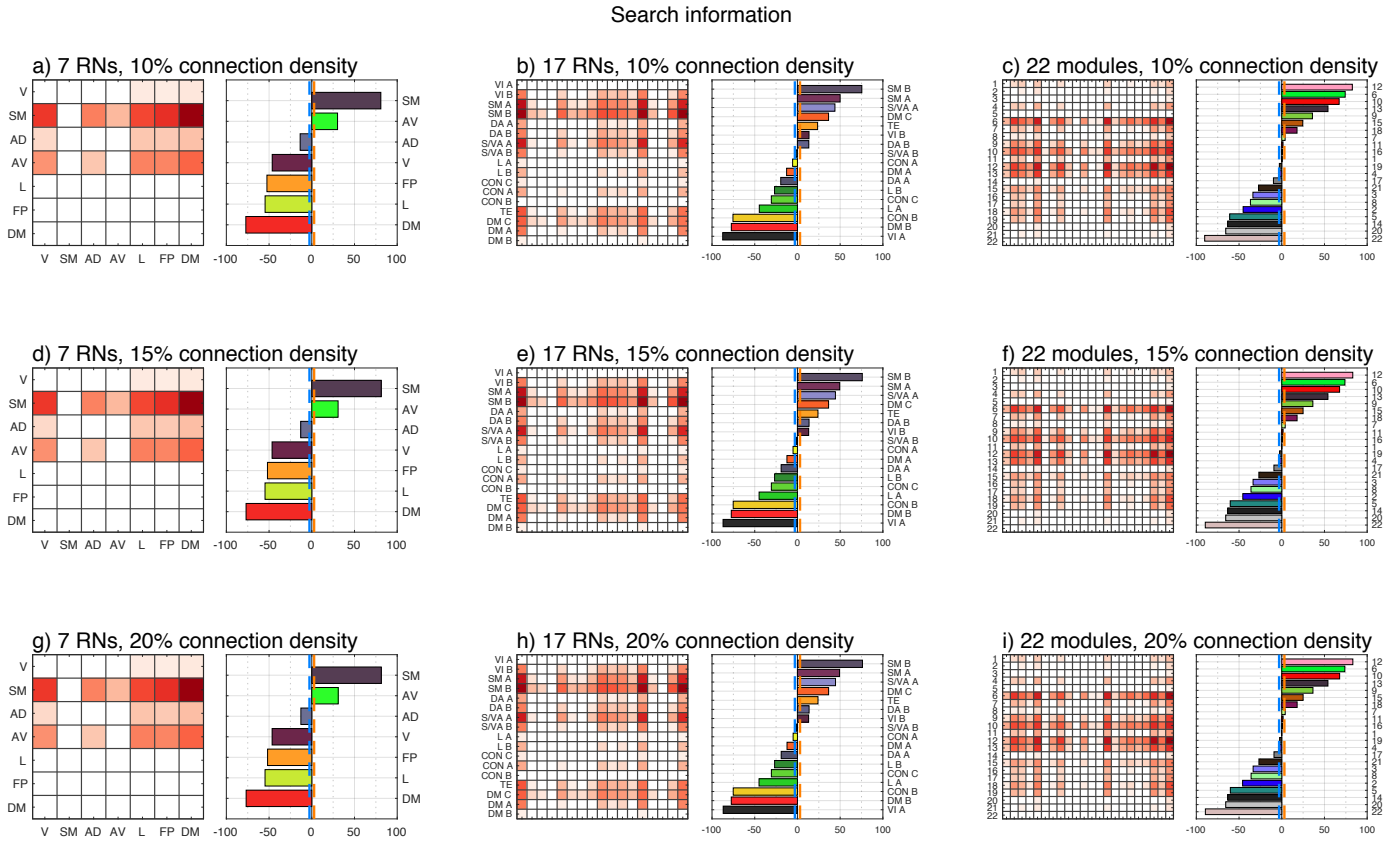


**FIG. S6.** Send-receive search information asymmetry of cortical subsystems for $M = 7, 17, 22$ and 10%, 15% and 20% connection density thresholds. Send-receive asymmetry matrices were thresholded to display only statistically significant values, while accounting for multiple comparisons. For ease of visualization and without loss of information (since $A(i,j) = -A(j,i)$), negative values were omitted. Thus, $A(i,j) > 0$ denotes that communication takes place more efficiently from $i$ to $j$ than from $j$ to $i$.